TAMPEREEN TEKNILLINEN YLIOPISTO
TAMPERE UNIVERSITY OF TECHNOLOGY

TIMO SAARINEN

HYBRID ORGANIC–INORGANIC NANOSTRUCTURES FOR SOLAR CELLS — A COMBINED EXPERIMENTAL AND COMPUTATIONAL STUDY

Master of Science Thesis

Supervisors and examiners:
Docent Terttu Hukka
Dr. Paola Vivo
Examiner:
Prof. Tapio Rantala
Examiner and subject approved by the Faculty Council of the Faculty of Science and Bioengineering in August 2015

ABSTRACT

Saarinen, Timo: Hybrid Organic–Inorganic Nanostructures for Solar Cells — A Combined Experimental and Computational Study
Tampere University of Technology
Master of Science Thesis, 56 pages
March 2016
Master's Degree Programme in Science and Engineering
Major: Physics
Supervisors and examiners: Docent Terttu Hukka, Dr. Paola Vivo
Examiner: Prof. Tapio Rantala
Keywords: hybrid organic–inorganic solar cell, bulk-heterojunction solar cell, solid-state dye-sensitized solar cell, perylene monoimides

Hybrid organic–inorganic photovoltaics (HOPVs) are emerging as an attractive solution to achieve cost-effectiveness and an acceptable performance. HOPVs offer several advantages over the traditional organic photovoltaics, namely the well-defined morphology, the high specific area of the inorganic–organic interface, and the high carrier mobility. However, further research and innovation are needed to understand how to engineer the organic–inorganic nanoarchitectures and achieve full control and the optimization of the nanomorphology.

This Thesis aims to offer a contribution in this direction by developing novel hybrid organic–inorganic solar cells via the assembling of highly-ordered functional layers at the interface between the inorganic and organic moieties.

Two main solar cell architectures were investigated in this work, namely bulk-heterojunction (BHJ) and solid-state dye sensitized solar cells (ssDSSCs). In both cases, a set of four perylene monoimide (PMI) antennas were assembled on metal oxides (zinc oxide, ZnO, or titanium dioxide, TiO_2) and tested as interlayer materials and sensitizers in BHJ solar cells and ssDSSCs, respectively. The final goal was to evaluate the effect of the introduction of the PMI antenna on the power conversion efficiency (PCE) of the photovoltaic devices.

Quantum chemical calculations were also carried out in order to find the highest occupied molecular orbital (HOMO) and the lowest unoccupied molecular orbital (LUMO) levels of the four PMIs applying the density functional theory.

In the BHJ experiments an overall improvement in the PCE was achieved, when comparing the performance of the reference solar cell, which did not contain PMI, to earlier results carried out in the same laboratory. However, the addition of the PMI interlayer did not enhance the solar cell performance.

The capability of PMIs to act as sensitizers was successfully verified in the ssDSSC experiments, by demonstrating the electron injection from PMI monolayer to the titanium dioxide. In fact, a 20-times increase in the PCE of the ssDSSCs was achieved thanks to the addition of the PMI. Furthermore, for two of the PMI cell-structures presented in this

work, the PCE values were comparable to those obtained for the device adopting a well-known and mostly used commercial ruthenium dye, N719. This suggests the beneficial use of the PMIs studied in this Thesis for ssDSSCs as potential replacements of the expensive rare metal ruthenium-containing dyes as modifiers of the TiO_2 surfaces.

TIIVISTELMÄ

Saarinen, Timo: Orgaanisten ja epäorgaanisten materiaalien hybridi-nanorakenteet aurinkokennoissa
Tampereen teknillinen yliopisto
Diplomityö, 56 sivua
Helmikuu 2016
Teknis-luonnontieteellinen diplomi-insinöörin tutkinto-ohjelma
Pääaine: Fysiikka
Tarkastajat: tutkijatohtori Paola Vivo, dosentti Terttu Hukka ja professori Tapio Rantala
Avainsanat: orgaanis-epäorgaaniset hybridiaurinkokennot, bulkkiheterolii-tosaurinkokenno, kiinteän olomuodon väriaineherkistetty aurinkokenno, pe-ryleenimonoimidit

Orgaanis-epäorgaaniset hybridiaurinkokennot, (engl. hybrid organic–inorganic photovoltaics, HOPVs) ovat tulleet tunnetuiksi houkuttelevana ratkaisuna aurinkokennotekniikassa kustannustehokkuuden ja hyväksyttävän suorituskyvyn saavuttamiseksi. HOPVs tarjoaa useita etuja verrattuna perinteiseen orgaanisen aurinkosähkötekniikkaan: tarkoin määritelty morfologia, orgaanis-epäorgaanisen rajapinnan suuri pinta-ala ja suuri varausten liikkuvuus. Lisätutkimusta ja uusia innovaatioita kuitenkin tarvitaan sen ymmärtämiseen, miten suunnitella orgaanis-epäorgaanisia nanorakenteita ja saavuttaa täysipainoinen nanomorfologian optimointi ja kontrolli.

Tässä työssä tavoitteena on osaltaan myötävaikuttaa em. tavoitteiden toteuttamiseen: on kehittetty uusia orgaanisten ja epäorgaanisten materiaalien hybridi-nanorakenteita asentamalla toiminnallisia kerroksia epäorgaanisen ja orgaanisen materiaalin rajapintaan.

Kahta tärkeintä aurinkokennoarkkitehtuurityyppiä tutkittiin tässä työssä: bulkkiheterolii-tosaurinkokennoa (BHJ) ja kiinteän olomuodon väriaineherkistettyä aurinkokennoa (ssDSSCs). Molemmissa tapauksissa neljää erilaista peryleenimonoimidikerrosta (PMI) testattiin metallioksidin (sinkkioksidi, ZnO tai titaanidioksidi, TiO_2) päällä välikerroksena (BHJ) tai herkistinaineena (ssDSSC). Lopullisena tavoitteena oli arvioida PMI-kerroksen vaikutusta valmistettujen aurinkokennojen hyötysuhteeseen (PCE). Myös kvanttikemiallisia mallinnuksia tehtiin molekyylien HOMO- ja LUMO-tasojen määrittämiseksi käyttäen tiheysfunktionaaliteoriaa.

BHJ-kokeissa havaittiin energiatehokkuuden paranevan suhteessa vertailukennoihin, jotka oli tehty ennen tätä työtä samassa laboratoriossa ja joissa PMI-molekyyliä ei ollut mukana. Kuitenkaan PMI-välikerroksen lisääminen ei tuottanut parannusta aurinkokennon suorituskykyyn.

Sen sijaan PMI-molekyylien käyttö herkistinaineena todettiin tässä työssä onnistuneeksi ssDSSC-kokeissa toteamalla elektronien siirtyminen PMI-kerroksesta titaanidioksidiker-

rokseen. Kahdella kokeissa käytetyistä PMI-molekyyleistä saadut PCE-arvot olivat samaa suuruusluokkaa kuin samassa kennorakenteessa kaupallisella väriaineella (N719) ja noin 20-kertaisia verrattuna kennoon ilman väriainetta. Tästä syystä tutkittuja PMI-molekyylejä voidaan pitää potentiaalisina vaihtoehtoina kalliille ja harvinaiselle rutenium-väriaineelle.

PREFACE

First of all I would like to thank Prof. Tapio Rantala for allowing me to carry out this Thesis work in cooperation with the Department of Chemistry and Bioengineering. I also thank him for all the guidance I received as an examiner of my Thesis.

Furthermore, I thank Docent Terttu Hukka, for giving me the opportunity to write this Thesis, including her valuable co-supervision and examination of this work, and the other supervisor and examiner Dr. Paola Vivo, for guiding and supporting during the experimental work and the writing process. I am also grateful to Adj. Prof. Alexander Efimov and Dr. Zafar Ahmed for providing me with the perylene molecules studied in this Thesis.

Finally, I also thank M.Sc. Outi Kontkanen and Dr. Mika Niskanen for valuable comments and Dr. Mika Niskanen also for carrying out the molecular modeling calculations.

Tampere, 20th January, 2016

Timo Saarinen

TABLE OF CONTENTS

ABBREVIATIONS AND SYMBOLS

Alq_3	Tris(8-hydroxyquinolinato)aluminium
AFM	atomic force microscopy
AM	air mass coefficient
B3LYP	hybrid functional Becke's three parameter and the Lee–Yang–Parr
BHJ	bulk heterojunction
BL	blocking layer
BnDT	benzodithiophene
CB	conduction band
CBM	conduction band minimum
CI	configuration interaction
CIGS	copper indium gallium diselenide
D–A	donor–acceptor
DFT	density functional theory
DIO	1,8-diiodooctane
DPV	differential pulse voltametry
DSSC	dye-sensitized solar cell
DZ	double-zeta basis set
EQE	external quantum efficiency
FF	fill factor
FTAZ	fluorinated 2-alkyl-benzo[d][1,2,3]triazoles
FTO	fluorine-doped tin oxide
GGA	generalized gradient approximation
GTO	Gaussian-type orbital

HF	Hartree–Fock
HMPER	*N*,*N*'-bis-2-(1-hydroxy-4-methylpentyl)-3,4,9,10-perylene bis(dicarboximide)
HOMO	highest occupied molecular orbital
HOPV	hybrid organic–inorganic photovoltaic
HTM	hole transporting material
IR	infrared
ITO	indium tin oxide
LDA	local density approximation
Li-TFSI	bis(tri fluoromethylsulfonyl)imide
LUMO	lowest unoccupied molecular orbital
N719	ruthenizer 535-bisTBA
NC	nanocrystal
NLO	nonlinear optical properties
OPV	organic photovoltaic
P3HT	poly(3-hexylthiophene)
P3OT	poly(3-octylthiophene)
PBE0	combination of the pure functional of Perdew, Burke, and Ernzerhof
PCBM	[6,6]-phenyl-C_{61}-butyric acid methyl ester
PCE	power conversion efficiency
PEDOT-PSS	poly(3,4-ethylenedioxythiophene)-poly(styrenesulfonate)
PMI	perylene monoimide
PV	photovoltaic
SAM	self-assembling monolayer
Spiro-OMeTAD	2,2',7,7'-Tetrakis-(*N*,*N*-di-4-methoxyphenylamino)-9,9'-spirobifluorene
ssDSSC	solid-state dye-sensitized solar cell

STO	Slater-type orbital
SV	split-valence basis set
tBP	4-*tert*-butylpyridine
TCO	transparent conductive oxide
TDDFT	time-dependent density functional theory
TZ	triple-zeta basis set
UV	ultraviolet
VB	valence band
VBM	valence band maximum
ZA75	2-octyl-1,3-dioxo-2,3-dihydro-1H-benzo[10,5]-anthra[2,1,9-def]isoquinoline-8,9-dicarboxylic acid
ZA87	2-octyl-1,3-dioxo-6-(pyrrolidin-1-yl)-2,3-dihydro-1H-benzo[10,5]anthra[2,1,9-def]isoquinoline-8,9-dicarboxylic acid
ZA96	9-octyl-5,13-di(pyrrolidin-1-yl)-1H-isochromeno[6',5',4':10,-5,6]anthra[2,1,9-def]isoquinoline-1,3,8,10(9H)-tetraone
ZA97	2-octyl-1,3-dioxo-6,11-di(pyrrolidin-1-yl)-2,3-dihydro-1H-benzo[10,5]anthra[2,1,9-def]isoquinoline-8,9-dicarboxylic acid

eV	electron volt
$E_{diff,ox}$	the difference in volts between the oxidation potential of ferrocene and the oxidation potential measured for the sample
$E_{diff,red}$	the difference in volts between the oxidation potential of ferrocene and the reduction potential measured for the sample
E_g	band gap
Φ_{SD}	Slater determinant
I	electric current
I_{sc}	short circuit current
J	current density

J_{sc}	short circuit current density
P	power
P_{in}	input power
P_{max}	power at maximum power point
R_s	resistance in series
R_{sh}	resistance in parallel, shunt resistance
V_{oc}	open circuit voltage

1. INTRODUCTION

The increase of the world population and economy has led to a rapid rise of the total worldwide energy consumption. It has been predicted that the energy request on earth would double until 2050 and triple till year 2100. Moreover, as a consequence of the combustion of fossil fuels, which pollutes the environment with harmful substances, the price of oil and gases is destined to rise remarkably and permanently. [1]

For filling the energy demand gap, one new power plant of a one GW per day would be needed. The increasing of the world energy demand, together with the fossil fuel depletion, has led to the search of new, green and renewable energy sources. Different possibilities include wind, solar power, hydroelectric and geothermal systems as well as exploiting tide or ocean currents. From biomass, fuels could be provided by methanol, ethanol, hydrogen, and methane (biogas). [2, p. 3] Solar energy is recognized as a secure and sustainable energy that can reduce carbon emissions [3].

The transition to a renewable energy economy would provide environmental benefits not measured in standard economic terms. It has been predicted that by 2050 global carbon dioxide (CO_2) emissions would be reduced to 75 % of their levels in 1985, provided that energy efficiency and renewables are widely adopted, and, such benefits could be achieved at no additional cost. [2, p. 3]

Exploiting solar energy among the many types of photovoltaic (PV) devices (like organic, inorganic, and hybrid cells) is, in principle, an abundant solution for energy problems for several reasons. First, the annual energy needed globally is only a small fraction of the solar radiation from the sun. Then, the photovoltaic devices are environmentally friendly. [4]

The power of solar radiation on the earth's atmosphere is 1.75×10^5 TW. If the irradiance could be converted into electric energy with a 10 % efficiency onto 1 % of the earth's surface (and taking 60 % transmittance through the atmospheric cloud cover as an example), it would provide a resource of 105 TW. This corresponds to four or five times the total planet energy needs estimated for 2050. Considering the surface of the earth, 1 % cover is a high demand. The power density of solar radiation is not very high even in bright days, consequently large areas are needed for solar power applications. Moreover, weather conditions also put a limitation on the use of the solar energy. For these reasons, solar energy can only be considered as a supplementary part of the energy production, and it is competitive only in some special applications. [2, p. 15]

PV-cells generate electric energy from sun light. The solar spectrum covers the wavelength range from ultraviolet to infrared, thus only 30 % of the incident light energy fits into the visible light range. Infrared waves are too weak to generate electricity, but the photons in ultraviolet and visible ranges have enough energy to generate charges. [5]

The first photovoltaic cell with silicon p-n junction technology was developed in 1954 at the Bell Laboratories in the United States. Since then, the efficiencies have increased from

6 % of the first cell to 20 %. Certain disadvantages, including toxicity and high costs of the high needed purity of silicon wafers, have led researchers to seek for a low-cost and environmentally friendly solar cell technology. A new photovoltaic cell, mimicking the principle of photosynthesis in plants, was developed in 1991 by O'Regan and Grätzel with an efficiency of from 7.1 % to 7.9 %. This cell was called a dye sensitized solar cell (DSSC). [4]

The dye in the DSSC has the same role as the chlorophyll in plants, *i.e.* it absorbs light and generates electron excitation. In this way DSSCs mimic nature's photosynthesis, although they do not store energy [6]. In natural photosynthesis, sunlight is converted efficiently into chemical energy. Mimicking this natural phenomenon with the help of synthetic molecular architectures is desirable for developing efficient solar energy converting systems. [7]

Solar cell technologies are divided into three categories:

- silicon-based solar cells (the first generation)
- thin-film solar cells (the second generation), including amorphous silicon cells, cadmium telluride cells (CdTe) and cells based on copper indium gallium diselenide (CIGS)
- solar cells using organic materials (small molecules or polymers) based on nanotechnology (the third generation).

The first generation still dominates the commercial market [8].

In this work a set of four PMIs was tested as sensitizers for ssDSSCs and as interlayer materials in BHJ solar cells. Quantum chemical calculations were carried out in order to optimize the geometries and calculate the electronic properties of the four PMIs applying the density functional theory. In chapter two the basic concepts concerning the working principles of solar cells and the roles of the different compounds in the solar cells studied in this work are given. In chapter three the experimental and computational details, together with a comprehensive presentation of the solar cells' fabrication and characterization, are presented. Results and conclusions are discussed in chapters four and five, respectively.

2. BACKGROUND

2.1 Organic and inorganic solar cells

Let us analyze which are the basic differences, when switching over from the silicon-based semiconductor industry to the use of organic compounds for the solar cell development. Organic photovoltaics (OPV) can provide electricity at lower cost than their inorganic counterparts. The main reason for this is that the manufacturing of solar cells can be executed using printing processes, which is possible, if a material is solution-processable. This allows a flexible photovoltaics technology using fast printing processes, simple machinery and abundant materials. Furthermore, the high absorption coefficients, typical of organic materials, allow the absorption of all the light at their absorption maximum wavelengths in a layer of a few hundred nanometers. [3] In fact, the absorption coefficient, which depends on the material and also on the wavelength of light which is being absorbed, determines the penetration depth of light of a particular wavelength into a material.

On the other hand, in organic solar cells the charge carrier mobility is low and, consequently, the energy conversion efficiency rate is lower, too [9]. The solar cell efficiency (also called power conversion efficiency, PCE) means the ratio of the electrical output of a solar cell to the incident energy in the form of sunlight.

The earliest organic photovoltaics were based on a single organic layer between two metal electrodes. With this structure only very low efficiencies were obtained, due to small exciton diffusion lengths and hence to the poor exciton dissociation. [1]

In a device consisting of two layers, a donor and an acceptor material, there is a planar interface, where charges are separated. This improves the function of the solar cell and, thus, the efficiency of the device. The exciton dissociation becomes possible through an energy difference large enough between the donor and acceptor layers. Thus, a proper alignment of the energy levels is needed. The bilayer is surrounded by two electrodes whose work functions have also to match the donor highest occupied molecular orbital (HOMO), and the acceptor lowest unoccupied molecular orbital (LUMO). This enables charge extraction at the respective electrodes. [1] The photo-generation taking place in a bi-layered solar cell is illustrated in Figure 2.1. The absorption of a photon may occur both in the donor and in the acceptor layer.

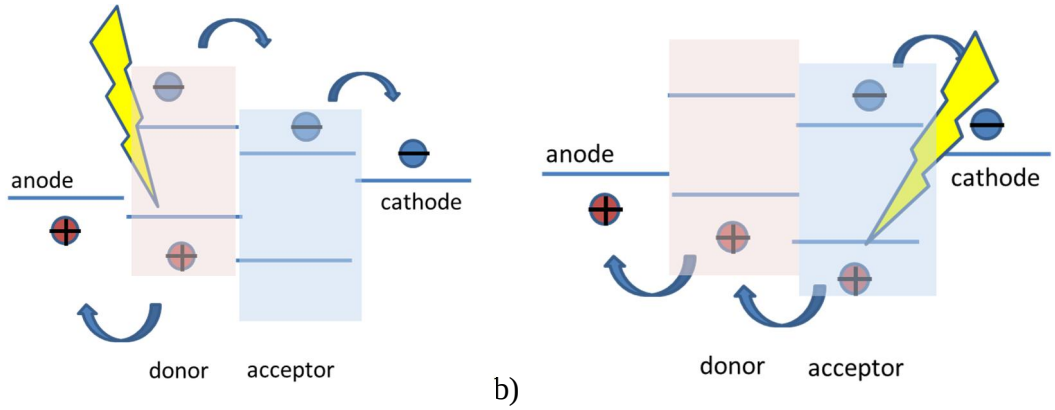

Figure 2.1. *a) Photo generation in the electron donor or b) in the electron acceptor. Redrawn from [10].*

In a bulk heterojunction (BHJ) the donor and acceptor materials are intimately mixed together, while in a bilayer heterojunction the layers are separated. The mixing of the materials leads to an increase of the active surface area and at the same time to a transition from a two-dimensional interface to a three-dimensional network. This also results in a multiplied probability for the impermanent excitons to reach the interface and dissociate.

In spite of the easy preparation of a bulk heterojunction — a bulk heterojunction solar cell may be prepared by solution processing techniques — the working mechanisms of a BHJ is complex and therefore not properly understood yet. The efficiency of a BHJ has reached values between 4 and 6 % in 2010 [1]. A little later (Scharber and Sariciftci, 2013) the power conversion efficiencies of BHJ solar cells were predicted to be 10–15 % [11]. The highest power conversion efficiency at the present has exceeded 11%. [12]

The basic structure of a BHJ can be considered as a blend system of many tiny pn junctions that are three dimensionally interconnected [5]. The bi-layer and bulk heterojunction structures are presented in Figure 2.2.

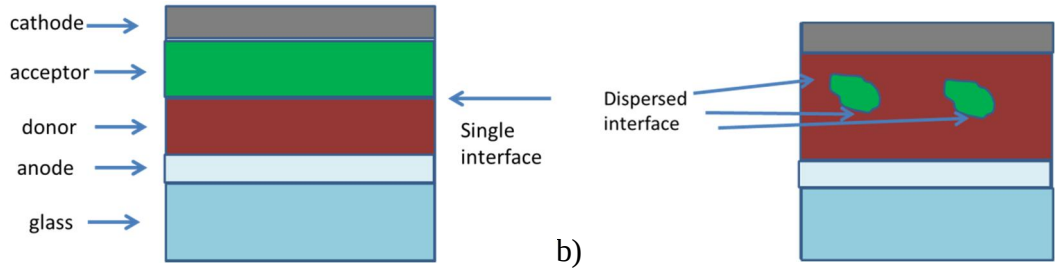

Figure 2.2*. a) Bi-layer structure, b) bulk heterojunction structure. Redrawn from [10].*

There are three types of polymer-based BHJ OPVs at the present: polymer–fullerene blends, polymer–polymer blends, and polymer–nanocrystal blends. [3]

The last generation of organic and hybrid organic–inorganic photovoltaics can be divided into three main cell types: flat-heterojunction cells, bulk-heterojunction cells, and dye-sensitized solar cells. Dye-sensitized solar cells, also called Grätzel-cells after Prof. Dr. Michael Grätzel, the pioneer in the field of dye-sensitized solar cells, are quite different from heterojunction cells both in their working principle and in the cell structure. [6] The

structure and operating model of a dye-sensitized solar cell will be presented in chapter 2.1.2.

2.1.1 Hybrid organic–inorganic solar cells

In hybrid organic–inorganic solar cells the organic materials, conjugated polymers or small molecules, absorb light and act as the electron-donors and hole transporting materials. The inorganic materials in hybrid cells are used as the electron-acceptors and electron transporters.

The power conversion efficiencies of devices containing organic materials have not yet been competitive with the 1st or 2nd generation (silicon) solar cells. Nevertheless, the hybrid organic–inorganic solar cells combine the advantages of both inorganic and organic materials, which make them suitable for several applications. The advantages of inorganic materials are stability and high carrier mobility, while those of organics are low fabrication cost, flexibility, facile solution processability, light weight, enhanced light absorption at a wide range of wavelengths and adjustable molecular structures for energy band. [11]

Hybrid solar cells have become of great interest, since the power conversion efficiencies have remarkably risen. The whole performance of the device is dependent on the electronic structure of the inorganic material included. One of the aims of the design of the device is to find the optimal electronic structure for an inorganic acceptor. Thus far**,** four material types, cadmium compounds (CdTe), silicon, metal oxide nanoparticles and low band gap nanoparticles have been explored**.** [10]

The operating principles of a hybrid solar cell and the corresponding energy diagram of the heterojunction are presented in Figures 2.3 and 2.4, respectively.

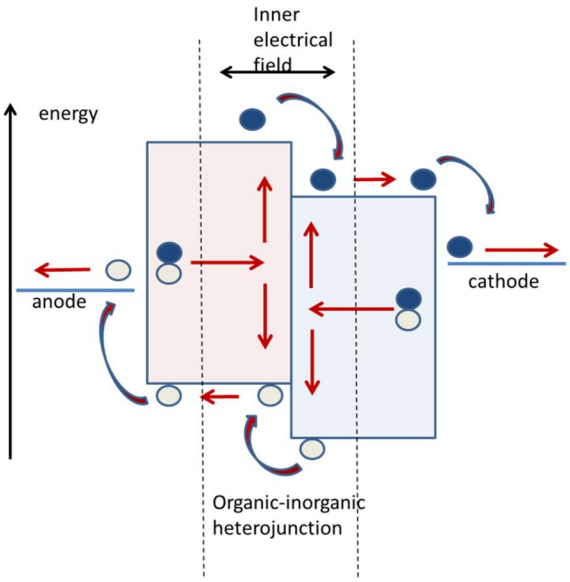

Figure 2.3. *Scheme of the operating principles of a hybrid solar cell, showing the dissociation of excitons and the charge transportation process. The electron and hole transfer processes are indicated with arrows. Redrawn from [13].*

In Fig. 2.3 the bound electron–hole combination (exciton) (electrons: blue circles, holes: empty circles), the dissociation process and finally the drift towards the electrodes are depicted by arrows. The straight arrows describe the inner electrical field and the curved arrows refer to the transitions of electrons and holes between donor and acceptor materials and further to the electrodes. This is discussed in more details in chapter 2.2.

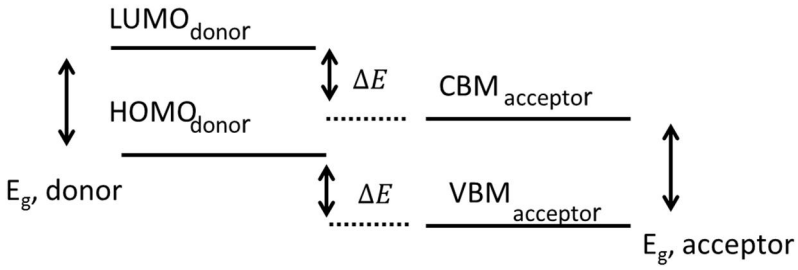

Figure 2.4. *General energy band diagram of the heterojunction formed in a hybrid solar cell Redrawn from [10]; E_g: band gap.*

Roughly, the HOMO level is to organic semiconductors what the valence band maximum (VBM in the picture) is to inorganic semiconductors and the same analogy exists between the LUMO level and the conduction band minimum (CBM).

The introduction of an inorganic component rather than an organic material offers a possibility to control the morphology at the heterointerface. However, there still remains a demand for the organic and inorganic phases to efficiently harvest sun light by covering the solar spectrum in a preferably complementary fashion. [14] Morphology will be discussed more in chapter 2.3.1.

2.1.2 Dye-sensitized solar cells

A dye-sensitized solar cell (DSSC), Grätzel cell, is a photoelectrochemical system consisting of a photoelectrode and a catalytic-electrode with an electrolyte between them. Its efficiency depends on many factors: the morphological properties of semiconductors, the spectroscopic properties of dyes, and the electrical properties of electrolytes. The first dye-sensitized solar cell, with an efficiency from 7.1 % to 7.9 %, was developed by O'Regan and Grätzel in 1991.[4] By 2009 the highest electrical conversion efficiency of DSSCs was 11.4% with a high absorptivity ruthenium sensitizer [15] and with porphyrin-sensitized solar cells with cobalt (II/III)-based redox electrolyte 12.3% under simulated air mass 1.5 global sunlight [16].

Dye-sensitized solar cells are based on wide band gap nanocrystalline titanium dioxide (TiO_2) semiconductors loaded with dyes. Ruthenium-complexes used as photo-sensitizers cause many problems like high cost, environmental problems, and difficult routes of synthesis. Pure organic dyes, compared with metal complexes, have higher absorption coefficients, which could save the amount of dyes used and reduce the thickness of the semiconductor film. [17]

Dye-sensitized solar cells' operating principle is based on an electrochemical reaction in which the active chemicals are constantly regenerated. TiO_2 nanoparticles, coated with the dye, absorb ultraviolet (UV) and visible photons causing an electron to be injected

into the conduction band of the TiO_2, whilst ions in the electrolyte pick up electrons from the other electrode to regenerate the dye.

The structure of a DSSC consists of a transparent glass sheet covered with a conductive indium- or fluorine-doped tin oxide layer, a mesoporous oxide layer (typically TiO_2), a monomolecular layer of dye (typically ruthenium complexes), an electrolyte (usually an organic solvent containing a redox mediator, such as iodide/triiodide couple) for the recovery of the dye and the regeneration of electrolyte itself, and a counter electrode (cathode), which is typically platinum, to catalyze the redox couple regeneration reaction and collect electrons. [18]

2.1.3 Solid-state dye-sensitized solar cells and perovskite cells

As for the dye-sensitized solar cell, eliminating expensive materials, like ruthenium and platinum, is difficult. Leakage and solvent evaporation in liquid-electrolyte based DSSCs is a problem, too, reducing stability in all weather conditions [4].

In a solid-state dye-sensitized solar cell (ssDSSC), in which the liquid electrolyte is replaced with a solid-state hole transporting material (HTM), the process of electron–hole generation and recombination is the same as in Grätzel cells.

Electrons are injected as a result of a photoexcitation from the dye into the conduction band of the TiO_2. The original state of the dye is thereafter restored by electron donation from the hole conductor. The hole conductor is subsequently regenerated at the counter-electrode. Then the circuit is completed via electron migration through the external load. [19]

Most sensitizers in ssDSSCs absorb only in the UV–visible region of the solar spectrum. Ideally a sensitizer would cover both visible and near infrared in absorption, because roughly 40 % of the irradiation can be found in the UV–visible region of the spectrum and around 60 % in the near infrared. The solar spectrum striking the earth differs from place to place and with the seasons depending on the earth's tilt. That is why scientists have agreed on standard conditions (AM 1.5 G) regarding tilt, temperature, albedo, and turbidity with one standard spectrum in order to make the test results of cells comparable.[1] The solar spectrum under 1.5 AM standard conditions is presented in Figure 2.5. [6]

[1] Albedo means an ability to reflect radiation and turbidity is the cloudiness or haziness of a fluid caused by large numbers of individual particles that are generally invisible to the naked eye.

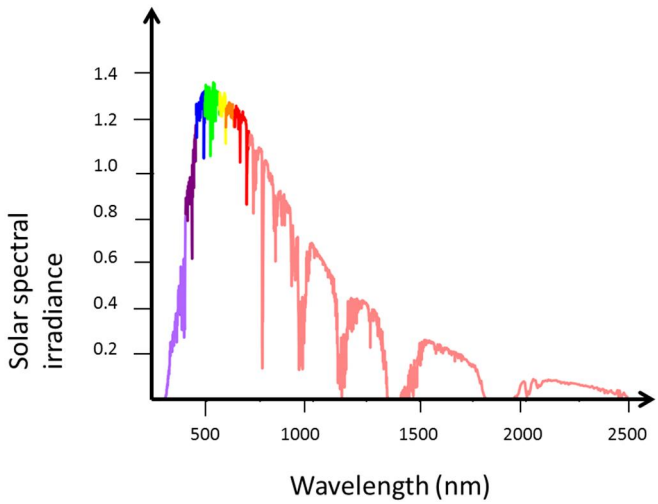

Figure 2.5. *Solar spectrum under 1.5 AM standard conditions. Redrawn from [6].*

Following photoexcitation in solution-processable organic and hybrid PV devices, the energetic cost of separating or transferring the bound charges from the absorber is high compared to conventional thin-film technologies. Inorganic–organic perovskites offer one way to diminish this adverse effect. [20] The exploitation of this new class of solar cells based on mixed organic–inorganic halide perovskites has grown very rapidly during 2012—present. Reported conversion efficiency values reach up to 17.9 % in early 2014. Currently the highest efficiency for a perovskite cell is 20.1 % [21].

Perovskite solar cells have got their names from the same type of crystal structure as calcium titanium oxide ($CaTiO_3$), known as the perovskite structure, the name referring to a mineral discovered by Russian mineralogist Perovski. This structure can be described with a formula ABX_3, where X is an anion and A and B are cations of different sizes [17]. A perovskite solar cell typically includes a perovskite absorber, most commonly a hybrid organic–inorganic lead or tin halide-based material, as the light-harvesting active layer.

Perovskites are easily fabricated and they have a strong solar absorption, a reasonably high carrier mobility as well as low non-radiative carrier recombination rates. There is also a possibility to capitalize on over 20 years of development of related dye-sensitized and organic photovoltaic cell. Negative aspects of perovskites are the toxicity of lead, which has been used as been a major constituent of all highly performing perovskite cells to date and degradation on exposure to moisture and ultraviolet radiation. [21]

2.2 Theoretical working principles of solar cells

2.2.1 Conversion of light into electricity

The main principles of a working hybrid organic–inorganic solar cell consist of several steps. At first light is absorbed by a dye; this generates bound electron–hole pairs, excitons. Excitons, in turn, may be thermally diffused into the donor–acceptor interface — or decayed to the ground state. Excitons arrived at the interface, then, rapidly dissociate with the help of the internal field. After this charge separation, the separated carriers are transported towards the electrodes and collected there. [13, 3]

This first step in the whole photocurrent process is the absorption of light, which may occur as well in the donor material as in the inorganic acceptor material. As a prerequisite for this there is a demand for the incident photons to have energies higher than the band gap of the organic and/or inorganic semiconductors. [13, 10]

Thus, the result of the absorption of light of appropriate wavelength in organic materials is the formation of excitons, in which the electrons and holes are coulombically bound — in contrast to inorganic materials, where free charges are formed. The binding energies of the excitons are around 0.4—0.5 eV. [3]

Due to the relatively large absorption cross sections of organic semiconductors, light absorption and exciton generation are favorable in hybrid organic–inorganic solar cells [13]. Absorption cross section is a measure for the probability of an absorption process, the probability of a certain particle–particle interaction, *e.g.* electromagnetic absorption.

The driving force for diffusion may be a difference in concentration or temperature. How far a concentration propagates in time is measured by diffusion length. In the case of excitons the diffusion length is the average length a carrier moves between generation and recombination. Excitons formed and diffused to the interface of the donor and acceptor material usually have diffusion lengths less than 20 nm in most organic semiconductors, whereas in silicon the diffusion lengths can be hundreds of nanometers. The low diffusion lengths in organic materials lead to quenching before carriers are formed. [13]

As far as the formation of carriers is concerned, the diffusion lengths determine the distance from the interface within which photoexcitation should take place. The advantage of a BHJ, compared to bi-layer structures, is the increased interfacial area by the mixing of the donor and acceptor materials. [10]

Exciton dissociation is to happen at the donor–acceptor (D–A) interface with the help of an inner electrical field built by organic and inorganic components with proper HOMO and LUMO energy levels. Although electron–hole pairs are generated by thermal energy in semiconductors, and thus can be broken with energies of the order of magnitude of 25 meV, excitons in organics need more energy to be broken. [13] The driving force to break strongly bound excitons is to be produced from the energy level difference between the LUMO of the donor and the conduction band edge of the acceptor materials [10].

In order to contribute to the photocurrent, the charge carriers produced by interfacial exciton dissociation must escape from recombination. Geminate pairs formed at the interface which fail to fully dissociate may recombine (geminate recombination) or also dissociated carriers generated by different absorption events (non-geminate recombination) (see Fig. 2.6).

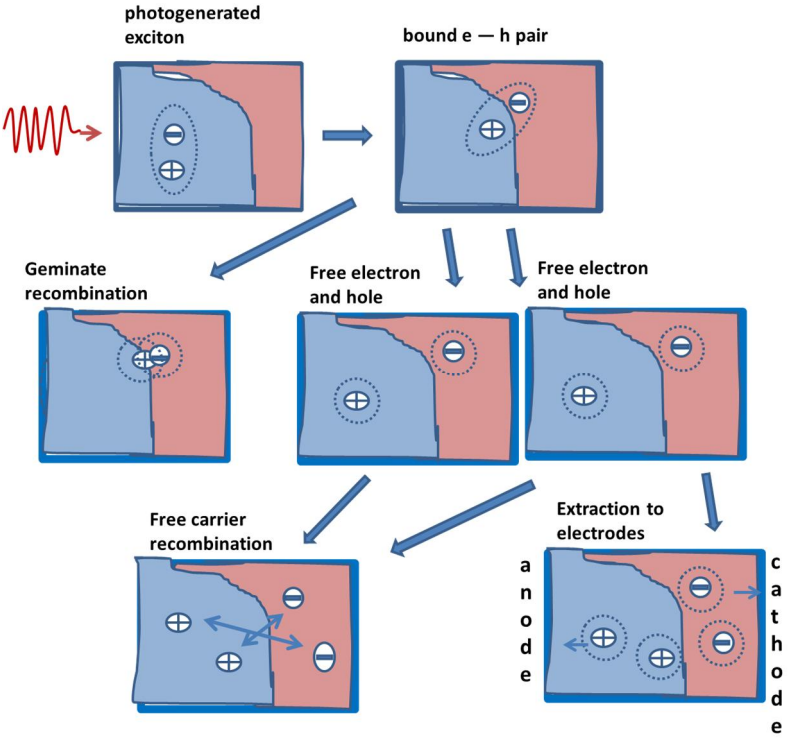

Figure 2.6. *Geminate and non-geminate recombination. The blue regions represent the donor material where the photoexcitation occurs and the acceptor material in this picture is drawn with purple.*

Hole and electron transporting to the electrodes occurs through the donor and the acceptor materials, respectively. Because the carrier mobility in organic materials is weak, (roughly 5 orders of magnitude lower than in silicon), the whole transportation process is a critical step in organic materials. [13] The mixing of donor and acceptor materials, which helps in exciton diffusion, is a hindrance in charge transport by way of increasing the opportunity of oppositely charged carriers to recombine [3].

This geminate decay of charge-transfer states is, however, less likely to occur in hybrid PVs, considering the large dielectric constant of inorganic nanocrystals (NC)[2]. Dielectric constant, relative permittivity, describes the force between two point charges in the material relative to vacuum. Consequently, the electron and hole dissociated from an exciton are relatively free from each other, and, geminate loss is not a dominant loss mechanism for hybrid PVs. [3]

Preferably, a direct path would be needed to guide charges to the electrode to contribute the photocurrent. In BHJ structures this may be hindered by parameters like morphology, mobility, and traps, which have to be optimized in order to achieve balance between charge separation and charge transport. [3] First, morphology denotes the study of how the shape and form of molecules affect their chemical properties, dynamic reconfiguration and interactions. Second, charge mobility must be large enough so that the carriers could be removed from the device before they recombine and, third, traps, which could stop

[2] A nanocrystal (NC) is a material particle having at least one dimension smaller than 100 nanometers, *i.e.* the particle is so small that quantum mechanical properties have to be taken into account.

charged carriers on their way transporting to the electrodes, may be morphological or energetic in nature: morphological “dead ends” do exist in devices based on nanodots as well as in those based on nanorods and the energetic trap states arise from defects or unpassivated nanocrystal surfaces. [3]

2.2.2 Performance characteristics

The operating principle of solar cells is expressed in this chapter by means of performance characteristics using the descriptions of the different stages of conversion of light into electricity presented in previous chapter and then, later in this chapter, by comparing a real cell to the ideal and describing the function of a solar cell by an equivalent circuit with ideal components.

The power conversion efficiency (PCE), η, of a photovoltaic device is defined as:

$$\mathrm{PCE} = \frac{J_{SC} \, x \, V_{OC} \, x \, FF}{P_{in}}, \qquad (1)$$

where J_{SC} *[mA/cm2]* = short circuit current density

V_{OC} *[mV]* = open circuit voltage

FF = fill factor, describes the ‘squareness’ of the *J–V* curve

P_{in} *[W/m^2]* = incident input power.

V_{OC} represents the difference of electrical potential between two terminals of a device when disconnected. It is directly proportional to the energy difference between the HOMO level of the donor and the LUMO level of the acceptor. [10]

$J_{SC,}$ the maximum photo-current density extracted from the device at short circuit conditions, is related to the external quantum efficiency (*EQE*), which is defined as

$$EQE = \eta_{abs} \; \mathrm{x} \; \eta_{diff} \; \mathrm{x} \, \eta_{diss} \; \mathrm{x} \; \eta_{tr} \; \mathrm{x} \; \eta_{cc}$$

$$= \frac{\text{photogenerated electrons collected at electrodes}}{\text{photons incident on the active layer}} . \qquad (2)$$

EQE is the product of the absorption yield of the device (η_{abs}), the ability of an exciton to diffuse (η_{diff}), the exciton dissociation yield (η_{diss}), the efficiency of charge carrier transport throughout the device (η_{tr}) and the efficiency of charge collection at the electrodes (η_{cc}). [10]

Considering formula (1), for input power, P_{in}, an international standard is used in defining fill factor (FF)

$$FF = \frac{J_{max} \, x \, V_{max}}{J_{SC} \, x \, V_{OC}}, \qquad (3)$$

where J_{max} and V_{max} are the maximum power point current density and voltage, respectively. The power conversion efficiency, PCE, can be written

$$\text{PCE} = \frac{P_{max}}{P_{in}} = \frac{I_{max} \, x \, U_{max}}{P_{in}} = \frac{FF \, x \, I_{SC} \, x \, U_{OC}}{P_{in}} . \qquad (4)$$

So, as a result, three major device characteristics completely determine the efficiency of the device. These three characteristics, J_{SC}, V_{OC} and P_{max} to be determined from the *I–V* curve, are illustrated in Fig. 2.7. P_{max} is the product of J_{max} and V_{max}. [10]

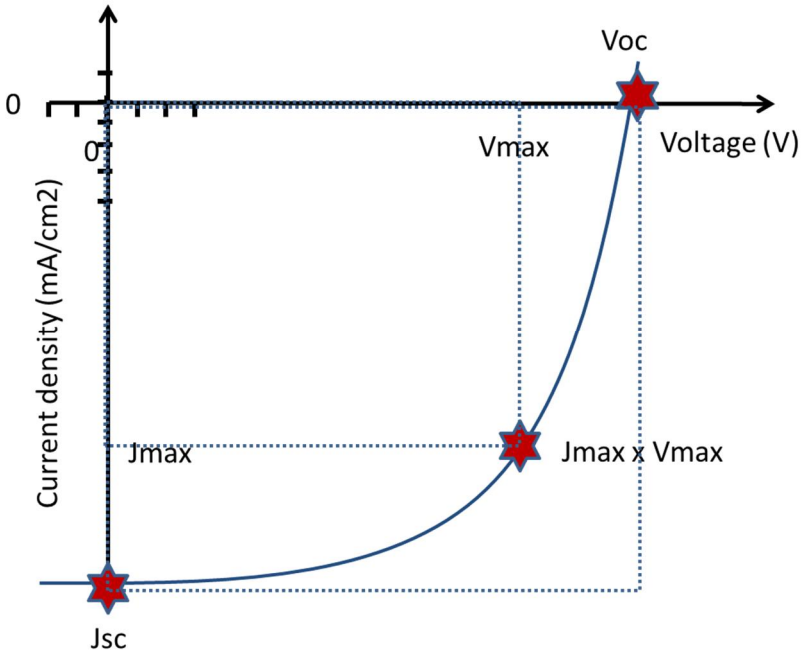

Figure 2.7. *Three major device characteristics which determine the* PCE. *Redrawn from [10].*

On the ground of equation 3, it is clear that fill factor is the relation of the areas of the rectangles formed as products of J_{max} and V_{max} and J_{SC} and V_{OC}, respectively.

Bulk heterojunction solar cells generally display low fill factors, because of non-ideal nanomorphology and a discrepancy between electron and hole mobility. The active layer–cathode interface can also play a major role in determining fill factor. [10]. *FF* depends on the product of the charge carrier mobility and lifetime of the bulk material, thickness of the active-polymer layer and on the morphology of the cathode–polymer interface. [22]

Comparing different solar cells in function certain parameters, like power conversion efficiency, are needed. These parameters can be derived from the current–voltage curve, *J–V* curve, in the dark and under illumination. Using the *J–V* curve it is possible to determine the highest possible current and voltage of the cell, fill factor, and in that way the power conversion efficiency of the cell. [5] While the current is zero, the solar cell delivers maximum voltage, and maximum current, when the voltage is zero.

Under dark conditions, there is no current at the short circuit condition, *i.e.* whilst the voltage is zero, but under illumination, on the contrary, the incident photons generate current and the minus current density in the 4th quadrant of the *J–V* curve indicates this photo generated current [5]. This is demonstrated in Figure 2.8.

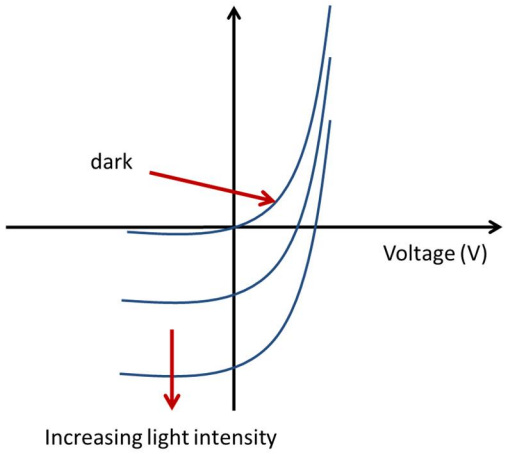

Figure 2.8. *Increasing light intensity, I–V curve.*

The function of a solar cell can be described by an equivalent circuit with ideal components. Two parasitic resistances, in series, R_s, and in parallel, R_{sh}, shunt resistance, are electrically equivalent to the dissipation effects in a real cell. These effects are caused by the resistance of the contacts and through leakage currents, *i.e.* the resistance of the cell material to current flow, particularly through the front surface to the contacts (R_s) and from leakage of current through the cell (R_{sh}). Both series and shunt resistances reduce fill factor, so smaller R_s and larger R_{sh} are required in an efficient PV cell. [5] In other words, R_s is the cell current limiting factor and it should be as small as possible, whereas R_{sh} is considered as a factor that inhibits recombination, and it should be as large as possible. [23] The circuit of a photovoltaic device with series and shunt resistances is in Figure 2.9.

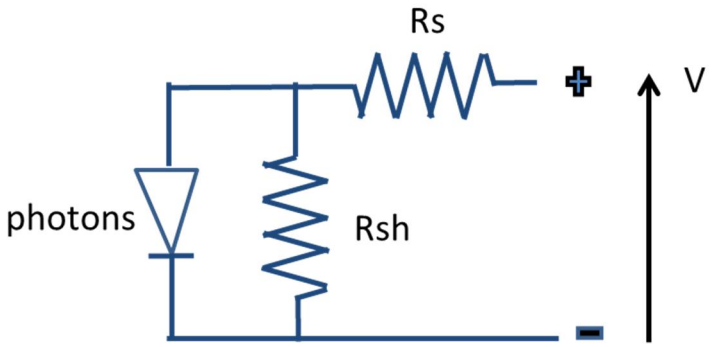

Figure 2.9. *The circuit of a photovoltaic device; R_s: series resistance, R_{sh}: shunt resistance.*

Both R_s and R_{sh} can be determined from the curve. R_s is dominant with high values of voltage ($V > Voc$) and then it is to be calculated as the reciprocal of the slope of the curve. R_{sh} can be calculated in the same way, but with small values of voltage ($V \approx 0$). [19]

The behaviour of a real diode will deviate from the ideal — the practical limit to fill factor is less than the ideal value of 1 — primarily as a result of recombination occurring at the junction, the D–A interface, for organic–inorganic hybrid solar cells. Deviations from the ideal case, and thus the shape of the *I–V* curve, can be characterized by the loss mechanisms of series and shunt resistance, as described in the previous paragraph. As for the series resistance, poor conductivity through the active layer and reduced charge carrier injection to the electrodes account for an increase in it (zero series resistance, $R_s = 0$, is ideal). [10]

2.3 Investigated compounds and their roles in the fabricated hybrid solar cells

The materials investigated in this Thesis, together with their role in the fabricated solar cell architectures, are introduced in this paragraph. However, it is important first to describe some fundamental concepts, such as the significance of film morphology, and the functions of donor and acceptor materials in solar cells, and to introduce perylene imides and their usage in solar cells. In the end of the paragraph, a summary of the suitable energy levels and an overview of the calculation of the electronic properties important for a working solar cell are presented.

2.3.1 Film morphology

This paragraph concentrates on the morphology of hybrid organic–inorganic nanostructures, consisting of inorganic semiconductor coupled with an organic dye.

The open-circuit voltage (V_{oc}), which is directly proportional to the energy difference between the HOMO level of the donor and the LUMO level of the acceptor, as stated in chapter 2.2.2, has a great influence on the power conversion efficiency of a photovoltaic device. The open-circuit voltage is significantly affected by the interfaces between active materials. This, consequently, leads to an increased need to investigate and understand interfacial microstructures in the photovoltaic systems. [24]

In hybrid solar cells a blocking layer (BL) between the front electrode and the mesoporous titanium dioxide is used to prevent short-circuits between the hole-conductor and the electrode. The conventional approach is to use a compact film of titanium dioxide, as a blocking layer, which has to be of optimum thickness: it has to cover the rough surface of the anode material completely while keeping it as thin as possible since the layer acts as an ohmic resistance itself. [25] Putting a blocking layer between the hole-transport material and the transparent conductive oxide material (TCO) increases the efficiency by three to four orders of magnitude in solid-state DSSCs. The blocking layer prevents the contact between the anode and the hole-transport medium but allows for the electron transport to the TCO. Typically, it consists of a compact layer of titanium dioxide with a thickness of about 100 nm. [25]

Another argumentation for engineering a compact blocking layer between TCO and TiO_2 is that holes in the HTM and TCO surface electrons recombination processes originates a remarkable current leakage path. The existence of the blocking layer leads to a drastic reduction of the back transfer recombination rate but letting the photo-extracted electrons to be efficiently collected. [26]

Except for recombining caused by titanium dioxide being directly in contact with the hole-transporting material — which is prohibited by a monolayer of dye — electrons gathered at the anode can recombine with holes in the donor-type material when these two materials are connected [25].

Then there are other ways to affect the nanomorphology of the solar cells:

A processing additive may improve the morphology, induce a faster charge generation, and balanced charge transport. 1,8-diiodooctane (DIO) has been used as such an additive in a BHJ cell consisting of benzodithiophene (BnDT) as a donor and fluorinated 2-alkyl-benzo[d][1,2,3]triazoles (FTAZ) as a acceptor together with $PC_{70}BM$ [27].

Also a relationship between the processing temperature and surface topography of TiO_2 films has been suggested [28] and an impact of the nanocrystal dimensionality on the polymer–inorganic nanocrystal hybrid blends [29].

The nanomorphology of hybrid organic–inorganic photovoltaics is better controllable than that of BHJ organic photovoltaic devices. The improved performance of optoelectronic devices as a result of engineering the organic–inorganic nanoarchitectures is evaluated mainly in terms of power conversion efficiency and stability. Even better control of the film morphology may also be obtained by controlling the orientation of the organic dyes on the surface of the metal oxide.

2.3.2 Donor and acceptor materials

In this chapter there is a description of the requirements of the donor and acceptor materials used in solar cells.

The desired traits of the donor material are its electronic composition properties and hole mobility. The appropriate values of the band gap and the HOMO and LUMO levels, with respect to the acceptor material, are of particular importance. Utilising a large portion of the solar spectrum, a relatively small band gap of the donor material is needed, simultaneously maintaining a sufficient offset in LUMO levels for excitonic dissociation. [10]

Efficiencies in bulk-heterojunction solar cells using a [6,6]-phenyl-C61-butyric acid methyl ester (PCBM) acceptor exceeding 10 % may be obtainable for an all organic device if certain design rules are used when choosing the donor material. It has been suggested that the band gap should be less than 1.74 eV and the LUMO level less than -3.92 eV, with respect to the vacuum level. [30]

Choosing the acceptor material requires close consideration to both electronic structure and additionally, physical constraints. One of the main advantages of inorganic semiconductor nanoparticles is the tunability of the band gap, as a result of modifications in the physical dimensions of the nanoparticle.

The ideal qualities have been predicted [31] using hybrid density functional theory, analyzing the electronic structure of inorganic acceptors. This inorganic acceptor was to be coupled with poly(3-hexylthiophene-2,5-diyl) (P3HT), which is the most commonly used polymeric donor: a compromise has to be done between increasing both V_{oc} and J_{sc}. To ensure good photon absorption, and thus high *Jsc*, the band gap of the acceptor material must be minimized so that more of the solar spectrum can be utilized. On the other hand, V_{oc} will be maximized by having a high lying conduction band edge in the acceptor material. An additional requirement for the acceptor material is a ground state offset of the acceptor valence band edge, with respect to the HOMO level of the donor material, to facilitate excitonic dissociation when light is absorbed in the acceptor material. [10] The ideal electronic requirements of an inorganic acceptor for hybrid solar

cells in a schematic diagram, according to the authors [31], are as presented in Figure 2.10. The ideal inorganic nanomaterial would have both a band gap of 1.5 eV and a HOMO level offset of 0.3 eV.

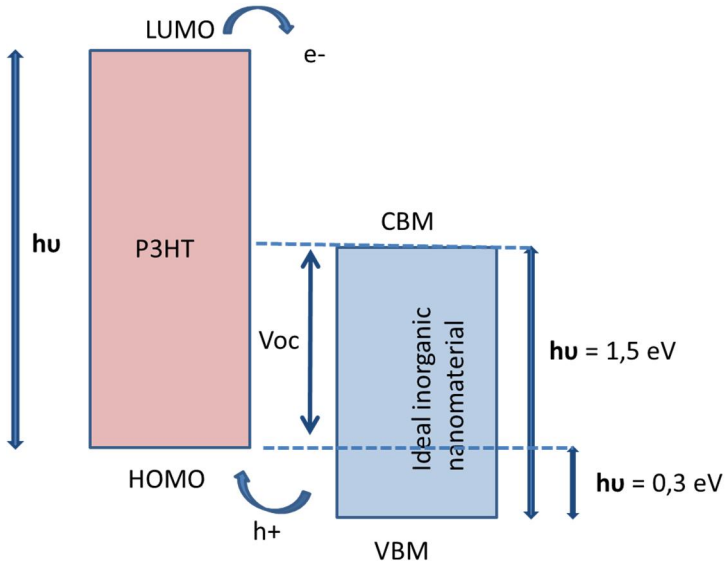

Figure 2.10. *Schematic illustration depicting the ideal electronic configuration for an inorganic acceptor material coupled with P3HT. Redrawn from [10]*

Considering the compromise between increasing both $J_{sc,}$ and V_{oc} mentioned above, low bandgap NCs could potentially increase the absorption and hence the photocurrent of the device, but at the same time the open-circuit voltage is to become sacrificed. For this reason some NCs with relatively wide bandgaps, *e.g.* CdS, ZnO, TiO_2, etc. have also been explored as the acceptor materials in hybrid PVs. [3]

In addition to the electronic structure some physical aspects are to be taken into account when choosing the acceptor material. These include solubility in a common solvent with the donor material, abundance and cost of the inorganic material, ability to achieve a balance between electron and hole mobilities and the success of the nanomorphology of the donor–acceptor phases. A compromise should then be made between these factors. [10]

Consequently, from the PCE point of view, the band gap of the acceptor material should be narrow to achieve large absorption and, at the same time, the diagonal band gap should be large enough, *i.e.* a high conduction band edge of the acceptor material is required, to maximize V_{oc}.

2.3.3 Perylene imides

Perylene imides are among the most stable organic compounds. Perylene derivatives have been used as commercial products and they are recognized as an important class of high-performance pigments. [32]

Perylene imides are n-type semiconductors and they (together with their derivatives) have been a research target for 100 years in the field of organic electronics. The perylene imide derivatives have been used in several types of organic photovoltaics: flat-, and bulk-heterojunction devices, as well as in dye-sensitized solar cells. By functionalizing

different positions on the perylene core, perylene imides with significantly different optical, electronic and morphological properties may be prepared. [32]

Using substituted perylene imides, the substitution pattern greatly influences the chemical and physical properties of perylene dyes. For example, when perylene derivatives are used as sensitizers in DSSCs, the molecule should have an anchoring group through which it can bind onto the substrate surface. Moreover, the presence of electron donating groups on the perylene core can increase the photoconversion efficiency. [33]

The perylene core has twelve functionalizable positions: the 3,4,9,10 positions, which are known as the peri-, the 1,6,7,12, known as the bay-, and the 2,5,8,11 known as the ortho-positions [32]. The functionalizable positions of the perylene core are depicted in Figure 2.11.

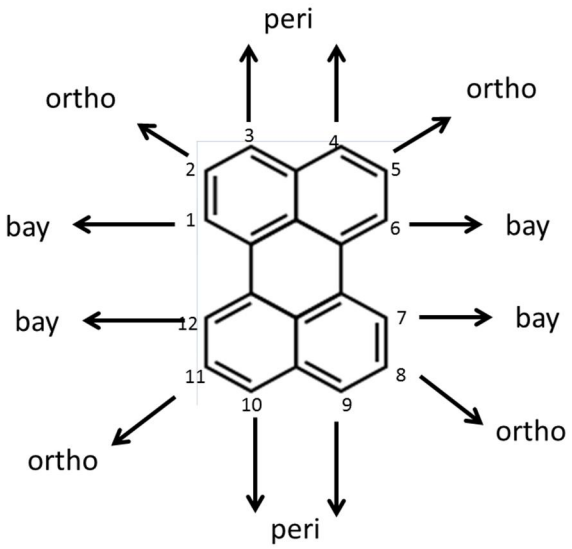

Figure 2.11. *Twelve functionalizable positions of the perylene core. Redrawn from [32]. [34]*

At first, the 3,4,9,10-diimides substitutions were intensively developed, nowadays, additional or exclusive bay-decoration as well as the asymmetric perylene monoimides or monoanhydrides are being investigated. The recent discovery of the ortho-functionalization finally becomes an interesting direction for research in the future as the 3rd generation of perylene derivatives. [32]

Perylene diimides (PDIs) represent one of the most widely studied classes of organic semiconductors with possible applications in photovoltaic cells and other fields of electronics. PDIs are n-type semiconductors and used as electron accepting materials in all-organic photovoltaic solar cells, whereas most organic conducting materials can be described as p-type semiconductors. Perylene monoimide dyes have been also used for DSSCs with overall conversion efficiency of 1.61 % and 2.6 %. [17]

PDIs are inexpensive and easily accessible materials with general photostability but suffer from poor solubility in common organic solvents. Synthesis of highly soluble PDIs is very important for the preparation of thin films to be used in photoelectronic applications. [17]

A synthesis of novel 7- and 7,12-substituted perylene derivatives, 7-pyrrolidinyl and 7,12-bispyrrolidinyl perylene monoimide monoanhydrides and their corresponding dicarboxylic acids, having strong electron donating groups in the bay-region and anchoring groups at peripositions, has been reported. Self-assembling monolayers (SAMs) were prepared over ZnO films and TiO_2 nanoparticles and part of the results of the studies of the authors suggest that these compounds can be good candidates for their potential use as sensitizers in DSSCs and related applications. [33] Self-assembly is a term that refers to the spontaneous organization of randomly distributed objects into a precise pattern due to local interactions [8].

Studies on perylene imides

Some studies on perylene imides in BHJ solar cells, ssDSSCs and DSSCs are introduced in the following paragraph.

Wang and Wang presented in 2008 a soluble perylene-derivative dye, *N,N'*-didodecyl-3,4,9,10-perylene tetracarboxylic diimide (PDI), to improve the photovoltaic performance of poly(3-hexylthiophene) (P3HT)/ZnO bulk heterojunction cells through blending with the composite. As a result of the incorporation of PDI in the P3HT/ZnO composite, the light absorption and exciton separation may be significantly improved. [35]

The idea here was to introduce dyes with broad absorbtion in the whole solar light spectrum into the photoactive layers in order to solve the problem arising from the limited performance of polymer-based devices. [35]

Perylene derivatives possess high electron affinity and high absorption coefficient (about 10 times higher than poly(3-hexylthiophene), P3HT). The dyes have been used as photo-sensitizer in TiO_2 solar cells with polythiophene as hole conductors. [35]

In the previous work of Wang and Wang, 2007, [36], the same compound was used to sensitize a P3HT/TiO_2 hybrid solar cell, but PDI was added on TiO_2 nanoparticles by direct mixing. In this architecture, heterojunction films containing P3HT, the same PDI and TiO_2, TiO_2 and P3HT were designed to act as the electron acceptor and donor and the PDI was used as a sensitizer to enhance the photon absorption. According to the results, the light absorption, exciton separation and photocurrent under white light were dramatically enhanced by incorporation of PDI in the P3HT/TiO_2 composite. Chemical structure of the PDI, *N,N'*-didodecyl-3,4,9,10-perylene tetracarboxylic diimide, used in these studies [35, 36] is depicted in Figure 2.12.

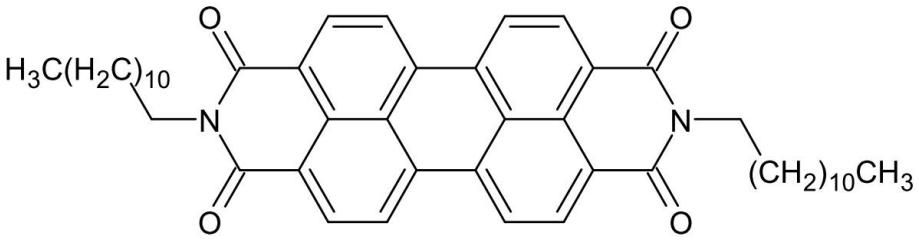

Figure 2.12. *Chemical structure of the PDI used by Wang and Wang. Redrawn from [35, 36]. [34]*

The mesoporous TiO_2 layer must be thinner in solid-state DSSCs than in liquid-electrolyte cells. Thus it is very important to use dyes with strong absorption and high surface coverage leading to maximized harvesting of the incident solar light. Organic dyes, particularly perylene monoimides, are excellent candidates due to their high molar extinction coefficients. [37] The molar extinction coefficient, or molar absorptivity, defines how strongly a substance absorbs light at a given wavelength, per molar concentration.

In a study by Howard et al., 2014 [37], the mechanism of charge generation in solid-state dye-sensitized solar cells using triarylamine-substituted perylene monoimide dyes (Figure 2.13) was investigated. According to the authors, the experiments demonstrate that photoinduded electron injection into the TiO_2 can only occur in regions, where Li+, from the commonly used bis(tri fluoromethylsulfonyl)imide (Li-THSI) additive salt, is present on the TiO_2 surface. As a result of incomplete surface coverage by Li+ some dye excitons cannot inject their electron into the TiO_2. [37]

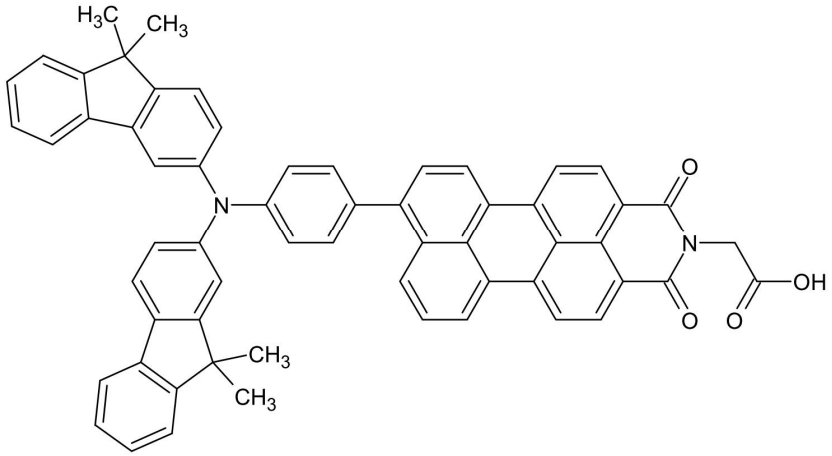

Figure 2.13. *Chemical structure of the triarylamine-substituted perylene monoimide sensitizer. Redrawn from [37]. [34]*

Erten-Ela and Turkmen reported in 2011 [38] on solid-state dye-sensitized solar cells using 2 perylene monoimide–monoanhydride dyes and the organic hole-transporting medium 2,2',7,7'-Tetrakis-(*N*,*N*-di-4-methoxyphenylamino)-9,9'-spirobifluorene (spiro-OMeTAD). The perylene imides used by the authors have an anhydride group (Figures 2.14 and 2.15); this group is a successful anchoring group, by the aid of which the mono imide–monoanhydride derivatives are immobilized onto TiO_2. [38]

A 0.046% overall conversion efficiency was reported under standard conditions obtained for a perylene imide derivative with PMI_1. [38]

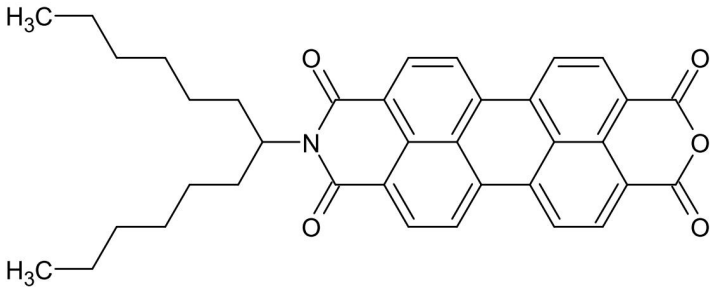

Figure 2.14. *N-(6-undecyl)-3,4:9,10-perylene tetracarboxylic acid-3,4-anhydride-9,10-imide, PMI_1. Redrawn from [38]. [34]*

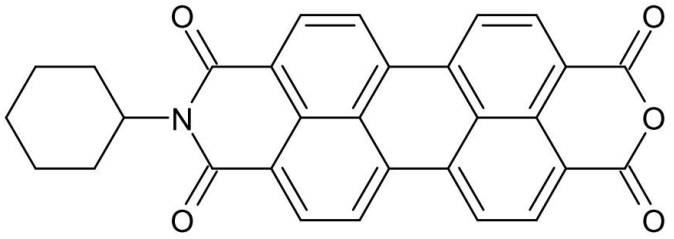

Figure 2.15. *N-(cyclohexyl)-3,4:9,10-perylene tetracarboxylic acid-3,4-anhydride-9,10-imide, PMI_2. Redrawn from [38]. [34]*

The side chain of a perylene imide dye affects the efficiency in solid-state dye-sensitized solar cell by preventing the charge recombination [38].

In an investigation by Zafer et al., 2004 [39], solid-state, dye-sensitized nanocrystalline TiO_2 solar cells based on perylene derivative dye, *N,N'*-bis-2-(1-hydroxy-4-methylpentyl)-3,4,9,10-perylenebis(dicarboximide) (HMPER, Fig. 2.16) with two different polythiophenes as hole conductors, poly(3-octylthiophene) (P3OT) and poly (3-hexylthiophene) (P3HT), respectively, were fabricated. HMPER adsorbs strongly onto the surface of nanocrystalline TiO_2 and inject electrons into TiO_2 conduction band upon absorption of light. They obtained quite similar results with P3OT and P3HT as for current density and open-circuit voltage. The results were compared with Ru-535 TBA-sensitized NC-TiO_2 cell prepared by using the same polythiophene derivatives. The major advantage of PDI derivatives over Ru-complexes is that their synthetic pathway is easier and basic chemicals are at lower costs. [39]

The overall energy conversion efficiency (PCE) of ≈0.02 % (light intensity 80 mW/cm^2, ITO/TiO_2 | PDI | P3HT/P3OT | LiF | Al configurations, ≈80 µA cm^{-2} short-circuit current, ≈0.7 V open-circuit voltage and FF ≈0.26) is quite low in comparison with DSSCs with liquid electrolyte. Reasons for this estimated by the authors may be a low contact area of hole conductor polymer and electron conductor nanocrystalline TiO_2 particles and/or HMPER being a poor sensitizer. [39]

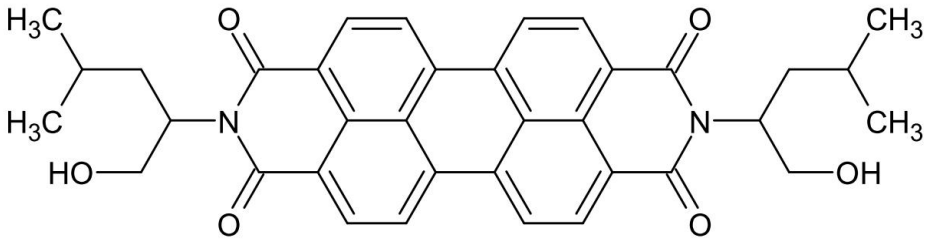

Figure 2.16. *N,N'-bis-2-(1-hydroxy-4-methylpentyl)-3,4,9,10-perylenebis(dicarboximide) (HMPER). Redrawn from [39]. [34]*

In a study by Fortage et al., 2008 [40], eight novel perylene imide derivatives (Fig. 2.17) were synthesized for dye-sensitized solar cells to determine the effect of the nature of electron donating substituents on the perylene core (ether or N-amino), the position of the carboxylic acid anchoring group and the presence of a fused benzimidazole moiety on the performances. They first investigated the effect of phenoxy (dyes 1—6) or piperidinyl substituents (dyes 7 and 8) at the bay positions of the perylene core in order to enhance the electron density on the perylene and make it a better electron donor. Another object for studying was the position of the anchoring group on the sensitizer and, third, the influence of the extension of the aromatic system by introducing a benzimidazole unit (dyes 2 and 4). [40]

The benzimidazole unit (dyes 2 and 4) extends the absorbance of the perylene imide to longer wavelengths. This effect is, however, lower than introducing charge transfer transition with N-amino substituents (dyes 7 and 8). [40]

Naturally, it must be taken into account that this study deals with DSSCs, and thus the conclusions based on the described substituents cannot be directly applied to ssDSSCs.

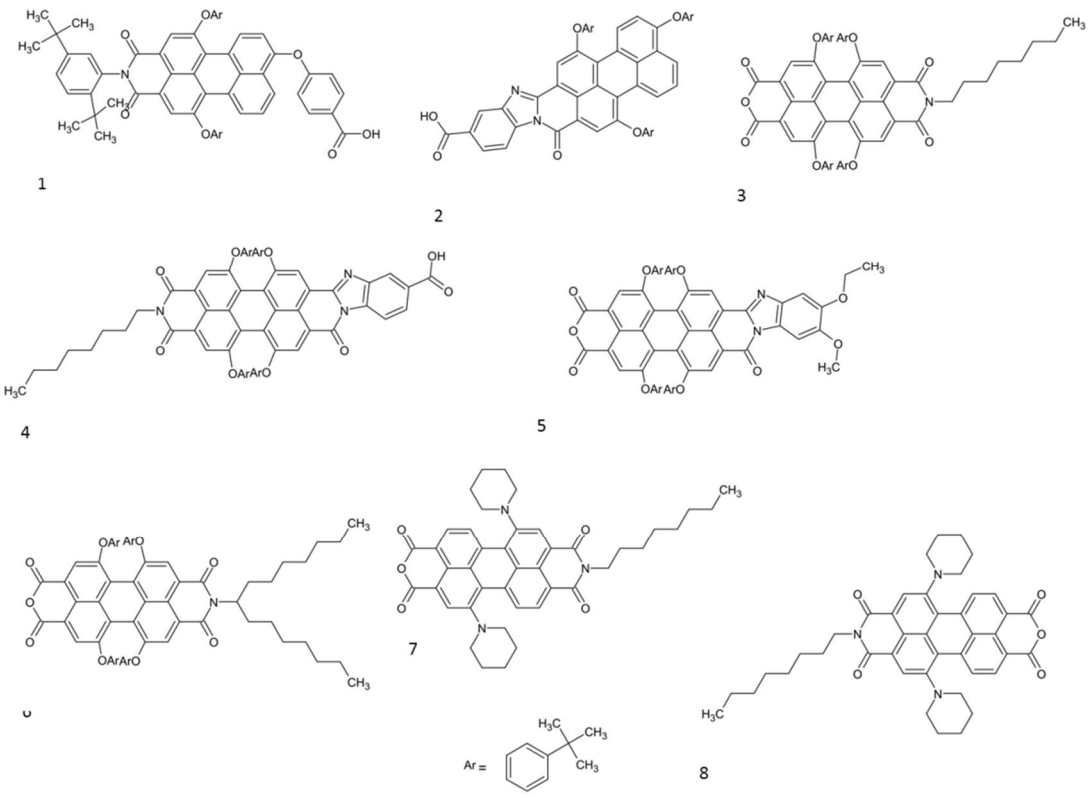

Figure 2.17. *Structures of the perylene imide sensitizers 1—8 prepared and investigated in the study by Fortage et al. Redrawn from [40]. [34]*

Shibano et al. reported (2007) [41] the synthesis of novel perylene imide derivatives with both electron-donating and bulky substituents. Using these perylene imides in dye-sensitized solar cells they reached power conversion efficiency 2.6 %, which is the highest value among perylene-sensitized TiO_2 solar cells. The authors underline that the perylene imides lack good electron-donating abilities. This makes it difficult to efficiently inject electrons from the excited perylene imide to the conduction band (CB) of the TiO_2 electrode and leaves the PCE values low. This has to be taken into account in the molecular design: multiple strongly electron-donating substituents (in this case two pyrrolidines) at the perylene core shift the first oxidation potential in the negative direction considerably and makes exothermic the electron injection from the excited singlet state to the CB of the TiO_2 electrode more exothermic, which leads to a more efficient photocurrent generation. The perylene imide synthesized by the authors, which reminds of one of the PMIs used in this Thesis (ZA96), is illustrated in Figure 2.18. [41]

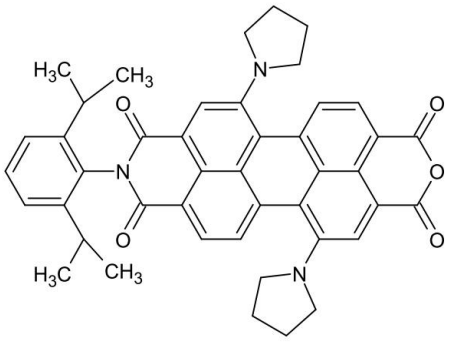

Figure 2.18. *Novel perylene imide derivatives with both electron-donating and bulky substituents synthesized for dye-sensitized solar cells. Redrawn from [41]. [34]*

2.3.4 Energy levels

When assembling films of different molecules in photovoltaic structures, the information on the energy levels (HOMO, LUMO) of the studied compounds is of paramount importance [1]. HOMO and LUMO level calculations are based on the oxidation and reduction potentials observed in the differential pulse voltametry (DPV) curves according to eq. 5 and 6 :

$$E_{HOMO} = -(4.8 + E_{diff,ox})\, eV \quad (5)$$

$$E_{LUMO} = (-E_{diff,red} + 4.8)\, eV, \quad (6)$$

where
- 4.8 eV is the oxidation energy of ferrocene
- $E_{diff,ox}$ is the difference in volts between the oxidation potential of ferrocene and the oxidation potential measured for the sample
- $E_{diff,red}$ is the difference in volts between the oxidation potential of ferrocene and the reduction potential measured for the sample. [23]

DPV is a widely used technique for the electrochemical measurements. The current difference is plotted as a function of potential and the current is measured immediately before each potential change. By sampling the current just before the potential is changed, the effect of the charging current can be decreased.

HOMO and LUMO energies are investigated by DPV in benzonitrile containing 0.1 M tetrabutylammonium tetrafuoroborate as a supporting electrolyte using glass platinum electrode as a working electrode, platinum wire as a counter electrode, and Ag/AgCl wire as a pseudo reference electrode. Ferrocene/ferrocenium (Fc/Fc+) couple was used as an internal standard reference to scale the measured potentials against the vacuum level. [33]

Interlayers are used in organic solar cells to better direct the holes and electrons in opposite directions, which results in increased current [42]. Figure 2.19 shows the conduction and valence bands of interface layers relative to the donor–acceptor active layer’s HOMO and LUMO levels.

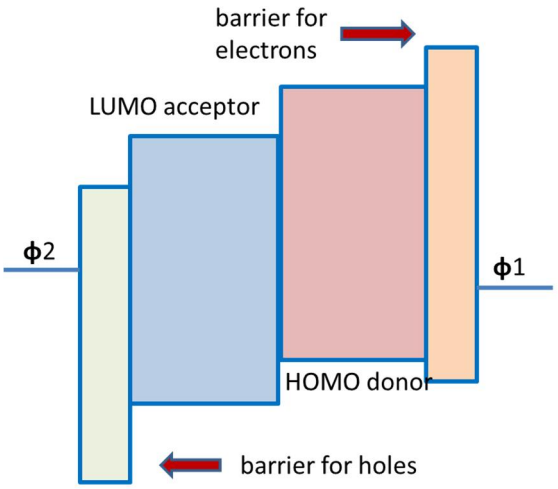

Figure 2.19. *The conduction and valence bands of interface layers relative to the donor–acceptor active layers' HOMO and LUMO levels.*

In most organic optoelectronic devices the front electrode is based on a transparent conducting oxide, such as indium tin oxide (ITO), that serves as the high-work-function positive electrode. This can be reversed by inserting a hole-blocking layer between the ITO and the active layer so that only electrons can reach the ITO, and the back electrode must become the hole-collecting positive electrode. [43]

In the case silver is used as the back electrode, its work function becomes higher through oxidation, the interface between silver and the organic layer oxidizes and silver oxide becomes a p-type semiconductor and a well-serving positive electrode. In figure 2.20a, ITO is the positive electrode and poly(3,4-ethylenedioxythiophene)-poly(styrenesulfonate (PEDOT:PSS) the electron blocking layer. In Figure 2.20b, where an inverted structure of a BHJ is depicted, zinc oxide (ZnO) is the hole-blocking layer. [43]

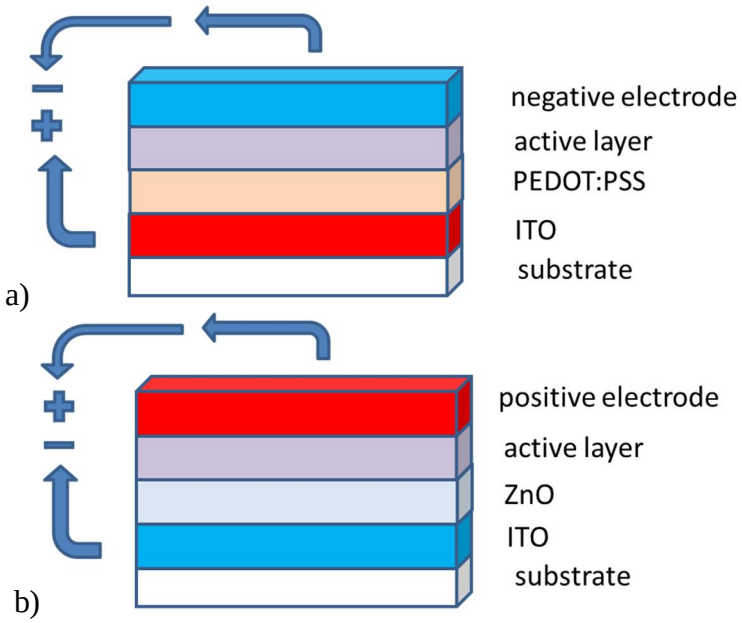

Figure 2.20. *(a) Normal geometry of a bulk-heterojunction solar cell. (b) Inverted geometry causes electrons and holes to exit the device in the opposite direction. Redrawn from [42].*

2.3.5 The calculation of the electronic properties of solar cell materials

The importance of the electronic properties for a working solar cell has been demonstrated in the previous chapters: a proper alignment of the energy levels between the donor and acceptor layers, for efficient exciton dissociation, appropriate work functions of the electrodes, which enables charge extraction and a charge mobility large enough so that the carriers could be removed from the device before they recombined.

The *ab initio* -methods, in which only quantum mechanics and basic physical constants are used, can be divided into two categories, based on Hartree–Fock theory (HF) or density-functional formalism. Density functional theory (DFT) is a natural manner of an approach for large systems, *e.g.* big molecules, Hartree–Fock theory for small systems. In DFT the basic starting point is that the energy of the system in the ground state in an external potential depend unambiguously on the electron density of the system. [44]

In DFT the energy is derived directly from the electron probability density, rather than the molecular wavefunction, thus drastically reducing the dimensionality of the problem. Density functional theory is rooted in quantum mechanics and therefore some elementary concepts from basic molecular quantum mechanics, centered around the Hartree–Fock approximation are needed. [45, p. 2]

The quantum chemical methods highly support the experimental results and can be combined with the results of electrochemical, spectroscopic, thermal, atomic force microscopy (AFM) and solar cell measurements [46].[3]

Density functional theory (DFT) transformed theoretical chemistry, surface science, and materials physics and has created a new ability to describe the electronic structure and interatomic forces in molecules with hundreds and sometimes thousands of atoms.

Density functional theory is a computational quantum mechanical modeling method used in physics, chemistry and materials science to investigate the electronic structure of many-body systems. With this theory, the properties of a many-electron system can be determined by using functionals, *i.e.* functions of another function, which in this case is the spatially dependent electron density. Density functional theory is a way to solve the electronic structure of matter in the presence of an external potential, the electron density being the basic variable. [44]

Using DFT it is possible to obtain information about polymer chain geometries, orbitals, HOMO and LUMO energies, electron affinities, ionization potentials and effective conjugation lengths. The systems are often too big for density functional theory, whereas semiempirical methods are often not accurate enough for such complex systems. Therefore, combining experimental and computational methods gives more details on the performance of the chosen polymers as donor materials. [46]

[3] Atomic force microscopy is a very high-resolution type of scanning probe microscopy with demonstrated resolution on the order of fractions of a nanometer, more than 1000 times better than the optical diffraction limit. Using an atomic force microscope, it is possible to measure the roughness of a sample surface at a high resolution.

Single electron approximation and the Hartree–Fock approach

In the single electron approximation the electron–electron interactions are not taken into account. Then, within a certain nuclear configuration, the wave function of n electrons can be separated into one-electron wave functions [44].

A one-electron image can be conserved when an average Coulomb potential of the other electrons, a Hartree potential, is added to the nuclear potential experienced by a single electron.

In the Hartree–Fock scheme the simplest, yet physically trustworthy approximation to the complicated many-electron wave function is utilized. It consists of approximating the *N*-electron wave function by an antisymmetrized product of *N* one-electron wave functions. This product is usually referred to as a Slater determinant (Φ_{SD}). [45, p. 9]

Variational principle is then used in order to find the best Slater determinant, the particular Φ_{SD}, which yields the lowest energy. The only flexibility in a Slater determinant is provided by the spin orbitals. In the Hartree–Fock (HF) approach the spin orbitals $\{\chi_i\}$ are now varied under the constraint that they remain orthonormal such that the energy obtained from the corresponding Slater determinant is minimal:

$$E_{HF} = min\ E[\Phi_{SD}]. \qquad (7)$$

The expectation value of the Hamilton operator with a Slater determinant can be derived by expanding the determinant and constructing the individual terms with respect to the various parts in the Hamiltonian:

$$E_{HF} = \langle \Phi_{SD} | \hat{H} | \Phi_{SD} \rangle = \sum_i^N (i \mid \hat{h} \mid i) + \frac{1}{2} \sum_i^N \sum_j^N (ii \mid jj) - (ij \mid ji) \ , \qquad (8)$$

where N is the number of the electrons in the system and the contribution due to the kinetic energy and the electron–nucleus attraction is

$$(i \mid \hat{h} \mid i) = \int \chi_i^*(\bar{x}_1) \left\{ -\frac{1}{2} \nabla^2 - \sum_A^M \frac{Z_A}{r_{1A}} \right\} \chi_i(\bar{x}_1)\, d\bar{x}_1 \qquad (9)$$

and the Coulomb and exchange integrals, respectively, which represent the interaction between two electrons, are

$$(ii \mid jj) = \int \int |\chi_i(\bar{x}_1)|^2 \frac{1}{r_{12}} |\chi_j(\bar{x}_2)|^2\, d\bar{x}_1\, d\bar{x}_2 \quad \text{and} \qquad (10)$$

$$(ij \mid ji) = \int \int \chi_i(\bar{x}_1)\, \chi_j^*(\bar{x}_1)\ \frac{1}{r_{12}}\ \chi_j(\bar{x}_2)\ \chi_i^*(\bar{x}_2)\, d\bar{x}_1\, d\bar{x}_2 \ . \qquad (11)$$

[44]

In the formula (9) M is the number of the nuclei in the system. The exchange interaction is a quantum mechanical effect between identical particles. The effect is due to the wave function of indistinguishable particles being subject to exchange symmetry, that is, either remaining unchanged (symmetric) or changing its sign (antisymmetric) when two particles are exchanged.

Basis sets

A basis set is a set of functions used to create the molecular orbitals, which are expanded as a linear combination with coefficients to be determined. One choice of basis functions are the Slater-type orbitals (STOs); then, in 1950, the introduction of Gaussian-type orbitals (GTOs) made ab initio calculations computationally feasible. Significant improvements were achieved by adopting a double-zeta or triple-zeta basis set (DZ or TZ basis set), in which each basis function in the minimal basis set is replaced by two or three basis functions. A split-valence basis set (SV basis set) is a compromise between the inadequacy of a minimal basis set and the computational demands of DZ and TZ basis sets. Each valence atomic orbital is represented by two basis functions while each inner-shell atomic orbital is represented by a single basis function. [44]

Electron correlation

The HF theory only considers the repulsion between the electrons as an average, it does not take the correlation interactions into account. Hence, a single slater determinant, Φ_{SD}, never corresponds to the exact wave function. Thus, owing to the variational principle, E_{HF} is necessarily always less negative than the exact ground state energy E_0:

$$E_C^{HF} = E_0 - E_{HF}, \tag{12}$$

where E_C^{HF} = the difference between these two energies, the correlation energy.

Electron correlation is the interaction between electrons in the electronic structure of a quantum system, mainly caused by the instantaneous repulsion of the electrons, which is not covered by the effective HF potential. As a consequence, the electron−electron repulsion term is too large resulting in E_{HF} being above E_0. [44] The simplest method which includes electron correlation via multiple Slater determinants is configuration interaction (CI), in which the exact ground-state or excited-state wavefunction can be expressed as a linear combination of all possible n-electron Slater determinants arising from a complete set of spinorbitals [47, 44].

Hohenberg–Kohn theorems

According to the first Hohenberg–Kohn theorem, the existence theorem, the ground state properties — also the external potential affecting the electrons, *e.g.* electron–nuclear attraction — of a many-electron system are uniquely determined by an electron density that depends on only three spatial coordinates. This theorem can further be extended to describe excited states in the form of the time-dependent density functional theory (TDDFT). The second Hohenberg–Kohn theorem, variational theorem, defines an energy functional for the system and proves that the correct ground state electron density minimizes this energy functional. [47]

Kohn–Sham orbitals

When the one-electron functions, so called Kohn–Sham orbitals are deployed, the energy of the ground state can be written in the form

$$E[\rho] = -\frac{\hbar}{2m}\sum_i^n \int \psi_i^*(\boldsymbol{r})\nabla_i^2\psi_i(\boldsymbol{r})\,d\boldsymbol{r} - \sum_i^n \int \frac{Z_i}{4\pi\varepsilon_0 r_1}\rho(\boldsymbol{r})\,d(\boldsymbol{r}) + \frac{1}{2}\int\int \frac{e^2\,\rho(\boldsymbol{r_i})\,\rho(\boldsymbol{r_j})}{4\pi\varepsilon_0 r_{ij}}\,d\boldsymbol{r}_i\,d\boldsymbol{r}_j + E_{xc}[\rho], \quad (13)$$

where $\rho(\boldsymbol{r}) = \sum_i |\psi_i(\boldsymbol{r})|^2$.

The first term represents the kinetic energy of the electrons, the second term is the energy of the electrons in the nuclear potential, third term describes the Hartree energy (the average potential of the rest of the electrons) and the last term contains the correlation and exchange energy, which depends on the electron density. [44]

In DFT formalism the one-electron image is preserved, although the correlation effects are taken into account. The density functional theory was preceded by Thomas–Fermi procedure for calculating the energies of the atoms from the charge density. [44]

LDA

The main source of error in DFT usually stems from the approximate nature of $E_{XC}[\rho]$ [43]. In the local density approximation (LDA) the electrons are treated as a uniform electron gas, *i.e.* el. density has the same value at every position. With this approximation the functional depends only on the density at the coordinate where it is approximated. In the generalized gradient approximation (GGA) LDA is improved by considering a non-uniform gas by making E_{XC} dependent on the local electron density and its gradient. GGA type functionals (*e.g.* PBE functional) are generally observed to yield a substantial improvement over the LDA type functionals. [48]

Examples of DFT calculations

For example, extensive DFT calculations have been performed to investigate the preferential adsorption of the organic dyes onto the {101} surfaces of anatase (one of the three mineral forms of titanium dioxide) TiO_2 nanoparticles theoretically (Diao et al., 2014) [24].

In another study (Mohr et al., 2015) [49], the geometries, electronic structures, polarizabilities and hyperpolarizabilities of some organic dye sensitizers, have been studied based on density functional theory. The DFT was treated according to hybrid functional Becke's three parameter and the Lee–Yang–Parr (B3LYP). The calculated results suggest that the three lowest energy excited states of the investigated dye sensitizers are due to photoinduced electron transfer processes. [49]

The electric polarizability is related to the systems response when distorted by an external electric field. Polarizabilities are crucial, because they determine the strength of molecular interactions, cross sections of different scattering and collision processes, and also the nonlinear optical properties (NLO) of the system. In this study by Mohr et al. the dye sensitizer hemicyanine system has been found to have a high NLO property, usually possessing high photoelectric conversion performance. This was the reason for calculating the polarizabilities and hyperpolarizabilities of the molecules, to investigate the relationships among photocurrent generation, molecular structures and NLO. [49]

The energy of the system can then be described in terms of a Taylor expansion relative to its field-free energy (*i*, *j* and *k* run over the Cartesian components). In this series development the terms of second and third order are the polarizability and the hyperpolarizability, respectively: [45, p.177]

$$E(\bar{F}) = E(0) + \sum_i \left(\frac{\partial E}{\partial F}\right) F_i + \frac{1}{2} \sum_i \sum_j \left(\frac{\partial^2 E}{\partial F_i \partial F_j}\right) F_i F_j + \frac{1}{6} \sum_i \sum_j \sum_k \left(\frac{\partial^3 E}{\partial F_i \partial F_j \partial F_k}\right) F_i F_j F_k + \cdots \text{, where} \quad (14)$$

E = the energy of the system,

$\bar{F}$ = electric field,

$\mu_i = \left(\frac{\partial E}{\partial F_i}\right)$ = the *i*'th component of the dipole moment vector $\vec{\mu}$,

$\alpha_{ij} = \left(\frac{\partial^2 E}{\partial F_i \partial F_j}\right)$ = *i,j*'th component of the polarizability tensor $\bar{\alpha}$,

$\beta_{ijk} = \left(\frac{\partial^3 E}{\partial F_i j k}\right)$ = the *i,j,k*'th component of the first hyperpolarizability tensor $\bar{\beta}$.

The derivatives of the energy are taken at zero field. [45, p. 177].

3. EXPERIMENTAL AND COMPUTATIONAL DETAILS

3.1 Description of the compounds

The four perylene monoimides used in this work will be presented in chapter 3.1.1, and their application as interlayers in BHJs and as sensitizers in ssDSSCs in chapter 3.2. The description of the other compounds used in the solar cells made is introduced in chapter 3.1.2.

3.1.1 Description of the photoactive molecules

The perylene monoimides (PMI) used in this work are presented in Figure 3.1. They are named in this work as follows: ZA75, ZA87, ZA96 and ZA97. The systematic names are below Figure 3.1. The third one (ZA96) represents a new family of perylene imides, where both the bay-substituents are located towards the anhydride cycle, the fourth one being its corresponding dicarboxylic acid [33]. The first PMI (ZA75) is not bay-substituted and the second one (ZA87) is bay-substituted from one side.

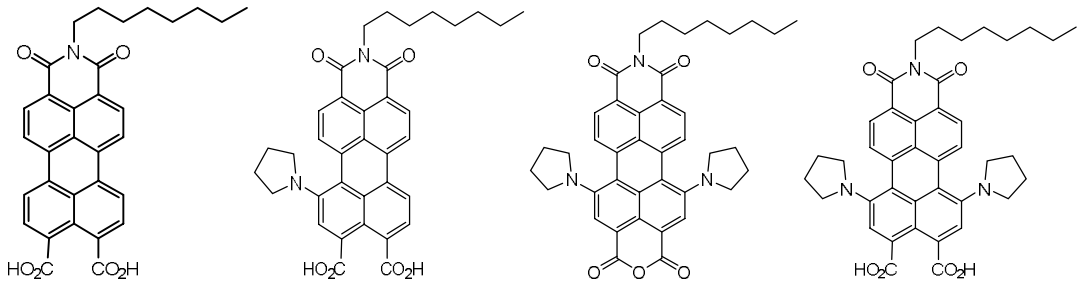

ZA75 ZA87 ZA96 ZA97

Figure 3.1. *Perylene monoimides used in this work. [33, 34]*

The systematic names of the compounds: [33]

- ZA75: 2-octyl-1,3-dioxo-2,3-dihydro-1H-benzo[10,5]-anthra[2,1,9-def]isoquinoline-8,9-dicarboxylic acid
- ZA87: 2-Octyl-1,3-dioxo-6-(pyrrolidin-1-yl)-2,3-dihydro-1H-benzo-[10,5]anthra[2,1,9-def]isoquinoline-8,9-dicarboxylic acid
- ZA96: 9-Octyl-5,13-di(pyrrolidin-1-yl)-1H-isochromeno[6',5',4':10,-5,6]anthra[2,1,9-def]isoquinoline-1,3,8,10(9H)-tetraone
- ZA97: 2-Octyl-1,3-dioxo-6,11-di(pyrrolidin-1-yl)-2,3-dihydro-1H-benzo[10,5]anthra[2,1,9-def]isoquinoline-8,9-dicarboxylic acid

3.1.2 Description of the other compounds

In this chapter the compounds used in the Thesis are described in detail: the metal oxides ZnO and TiO_2 as acceptor materials, the fullerene derivative PCBM as electron acceptor in BHJ cells (Fig. 3.2), the polymer poly(3-hexylthiophene-2,5-diyl) (P3HT) as electron donor and hole transporting material in both BHJ and ssDSSC cells (Fig. 3.3), and, finally, 2,2',7,7'-tetrakis-(*N*,*N*-di-4-methoxyphenylamino)-9,9'-spirobifluorene (spiro-OMeTAD), as hole transporting material in ssDSSCs (Fig. 3.4).

Zinc oxide, which has widely been used in hybrid organic–inorganic solar cells, is a wide band gap semiconductor with an energy gap of 3.37 eV at room temperature. Zinc oxide is stable in air, it is easily synthesized and it has a good light transmittance. [50, 13]

Titanium dioxide has also been extensively used in photovoltaic research due to its high chemical stability, low cost, non-toxicity, strong photocatalytic activity and high photoelectric conversion efficiency [13]. Titanium dioxide possesses the ability to form vertically aligned oxide nanostructures, which can be engineered so that the physical dimensions allow for optimization of a large donor–acceptor interfacial area. The wide band gap (a typical characteristic of oxide compounds) is not, however, desirable for use as an inorganic acceptor and leads to negligible absorption contribution in the visible spectrum. However, the position of the conduction band edge, which forms a heterojunction with the appropriate polymeric materials, yields a maximum obtainable V_{oc} which is quite similar to that of PCBM (Fig. 3.2). [10]

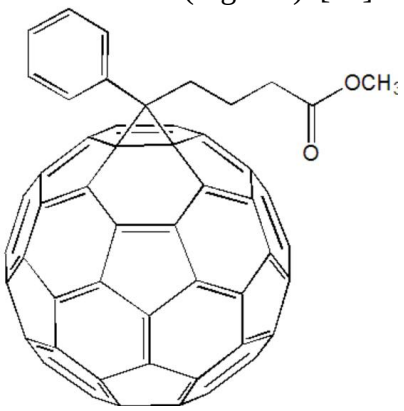

Figure 3.2. *Schematic presentation of the chemical structure of PCBM, [6,6]-phenyl-C_{61}-butyric acid methyl ester.*

Fullerene molecule is able to accept up to six electrons in solution, because of its electronegativity, and it is a good electron-acceptor compared to other organic molecules [1]. The disadvantage of polymer:fullerene devices is that the fullerene absorption is poor in the solar spectrum range [3].

P3HT is used as an electron donor and hole transporting material. It has a key role in the performance of the solar cells, due to its absorption in the central part of the visible spectrum — it absorbs a wide part of the visible region, between 400 and 650 nm (Fig. 3.3). [1]

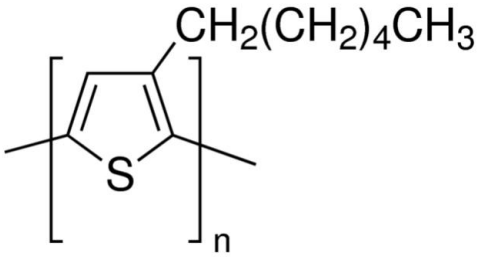

Figure 3.3. *Schematic presentation of the chemical structure of P3HT.*

Spiro-OMeTAD is a wide band gap p-type organic hole-conductor [20]. The spiro-OMeTAD molecule is depicted in Figure 3.4.

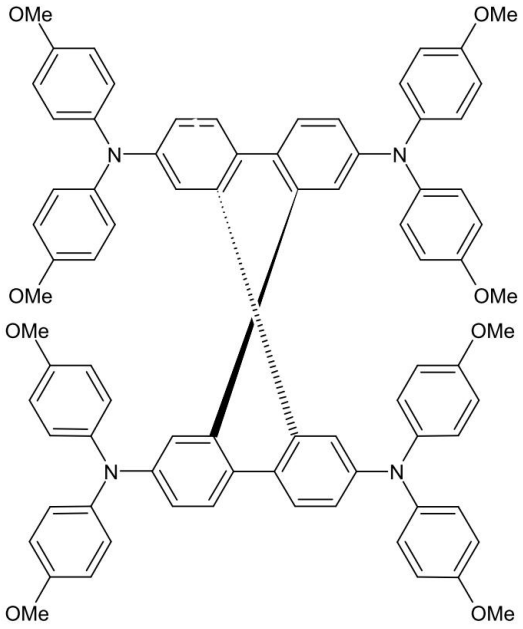

Figure 3.4. *Schematic presentation of the chemical structure of Spiro-OMeTAD. [34]*

In this work, novel organic dyes are used as sensitizers in ssDSSCs. They are placed between the titanium oxide and the hole transporting material. The dye is added because of a too wide energy gap of TiO_2 and the insufficient energy of the sunlight to form electron–hole pairs**.** Commonly, ruthenium dyes are adopted to this aim in ssDSSCs. However, ruthenium dyes are expensive (price varies from 200 to 2000 €/g), toxic, and of a limited availability. Thus, there is a need to find alternative organic dyes to replace those containing ruthenium.

In this work, a commercial dye, ruthenizer 535-bisTBA (N719), one of the best ruthenium dyes for the sensitization of titanium dioxide, was used as sensitizer in reference cells for comparison.

3.2 Experimental details

In this paragraph, a description of the structures of the investigated solar cells, as well as the deposition methods of the compounds used, are presented. Both BHJs and ssDSSCs were built and tested in the experiments. At first, the compositions of the bulk heterojunction solar cells, the characterization of the different layers and the preparation of the cells are introduced. Thereafter, the solid-state dye-sensitized solar cells made are

presented in the same way. Third part of this chapter includes the characterization of the solar cells built by means of defining certain parameters describing the function of the cell.

3.2.1 Bulk-heterojunction (BHJ) solar cells

The substrates on which the cells were built were made of glass coated with a transparent conducting indium tin oxide (ITO). ITO is a ternary composition of indium, tin and oxygen in varying proportions. It is the most widely used transparent conducting oxides because of its electrical conductivity and optical transparency, as well as the ease of deposition as a thin film.

ITO has a wide band gap of 3.2—4.0 eV, which covers 85 % of the solar spectrum. Thus, the active layer gets the opportunity of absorbing light of a large wavelength range. [19] Furthermore, bulk tin oxide, SnO_2, has a carrier mobility, which is 100 times that of TiO_2 — making it more suitable to high performance electronic devices [51].

To prevent short circuit when contacting the metal top-cathode, part of the ITO was removed from the plate by etching with aqua regia. The etching process takes place on clean substrates, patterned with tape as in Figure 3.5. After taping, the plates were covered with nail polish — two layers, one for 30 minutes, and the other overnight — and then, after tape removing, dipped in Milli-Q H_2O:HNO_3:HCl, 5:0.4:4.6 solution for 7 minutes to remove ITO from the white regions in the picture. In the end of this treatment the acid was neutralized by isopropanol and the nail polish removed by acetone. The plates were cleaned in sonicator with Milli-Q for 30 min, acetone for 1 hour and methanol for 1 hour and then dried in a vacuum at 150 °C for 1 hour.

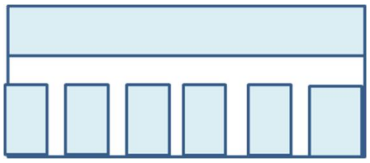

Figure 3.5. *A patterned ITO plate. White regions are of glass and the blue ones of ITO.*

The inverted structure of a bulk heterojunction solar cell (chapter 2.3.4) can be accomplished by using zinc oxide as the hole-blocking layer [43]. A zinc oxide interlayer between ITO and the photoactive layer efficiently collects electrons from the photoactive P3HT:PCBM layer to the ITO direction [23].

The ZnO layer was fabricated by thermal conversion of a spin-coated film from a chemical precursor solution of zinc acetate. The resulting ZnO layer is nanocrystalline in structure. A stock solution for zinc oxide precursor was prepared at first: 96 % 2-methoxy ethanol and 4 % ethanolamine. Then 50 mg/ml zinc acetate was dissolved in the 2-methoxy ethanol/ethanolamine mixture. The solution was heated and stirred for 2 hours at 70°C and then settled down overnight.

Before making the ZnO layer the ITO plates were cleaned in a plasma cleaner (Harrick Plasma Cleaner PDC-23G) for 10 minutes. The ZnO layer was made by spin coating: on the ITO plate 185 µl of the solution prepared with 2000 rounds per minute (rpm) for 1 minute. In the end the solvent was evaporated in the oven of 300 °C twice, rinsing the substrates between them with milli-Q water, ethanol and acetone.

The investigated PMIs were deposited as a self-assembled monolayer (SAM) between ZnO layer and the polymer–fullerene blend. Self-assembling monolayers (SAMs) of the PMIs were prepared in a single step. The substrate plates were annealed at 150 °C for 1 h prior to the deposition, for moisture removal. Then the substrates were cooled down at room temperature and blown with N_2 flow and immersed in 0,11 mM (or 0,30 mM) solutions of the PMI; a solution of ZA75 and ZA97 in ethanol, ZA87 in 3:1 ethanol:chloroform and a solution ZA96 in 1:1 toluene:ethanol.

The solutions were kept under stirring and heating immediately prior to the deposition to improve solubility as follows:
- ZA75: 500 rpm, 70 °C for 90 minutes
- ZA87: 500 rpm, 70 °C for 60 minutes
- ZA96: no stirring, 80 °C prior to the deposition
- ZA97: no stirring, no heating

Immersion times:
- ZA75: 24 hours
- ZA87: 3 hours
- ZA96: 24 hours
- ZA97: 3 hours.

After taking the substrates out, they were rinsed a few times by dipping into the solvent they were made in, and finally dried under N_2 flow.

It has been demonstrated that in the active layer blend of donor–acceptor pair P3HT:PCBM the natural tendency of P3HT to crystallize is disturbed by the addition of PCBM. Annealing however improves the crystallinity, resulting in a higher mobility of the holes in P3HT. [52]

As to the lifetimes of solar cells based on P3HT:PCBM bulk-heterojunctions, it has been showed that polymer solar cells, having a good light stability, can survive over one year of outdoor exposure without performance losses [43].

The organic P3HT:PCBM layer was prepared with mass ratio 1:0.8. The P3HT and PCBM solutions were prepared separately and stirred at 50 °C, 500 rpm overnight. The next step was combining the solutions, then bath temperature to 70 °C, 300 rpm, stirred for 4 h and then removed to 50 °C, 500 rpm overnight. Spin coating on the substrates was done with 190 μl of the solution and 600 rpm for 5 minutes.

Behind the silver cathode there is a thin layer of aluminum-tris-quinolate (Alq_3) as a buffer layer, to protect the active layers from the evaporation of the anode (Figure 3.6) [1].

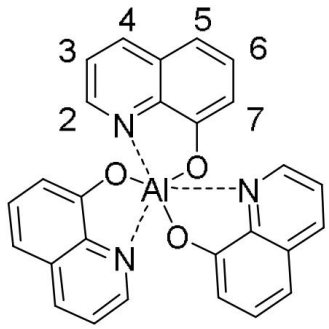

Figure 3.6. *Chemical structure of Alq_3.*

The buffer layer, which is an anode buffer layer in this work, because of the inverted solar cell structure, should strengthen the propagation of the holes to the anode by raising the work function of it. The buffer layer is also supposed to prevent electrons from arriving at the anode and to be thermally and photochemically stable. [53]

Choosing the metal electrode it is important to take the work function of the electrode into account in order to separate the charges formed in the interface. The work function of the ITO is about 4.7 eV; so, a metal with a work function higher than that acts as an anode in a solar cell (inverted structure). [19] The work function of pure Ag, 4.3 eV, is changed in air as Ag is oxidized and the work function of the formed silver oxide (AgO) is close to 5.0 eV [23].

The vacuum thermal evaporation is a common method for both organic and inorganic thin film depositions, which ensures smooth and homogenous films with controllable layer thickness. The source material is evaporated in high vacuum, 10^{-6} mbar, and the vapor particles travel to the substrate, where they condense back to the solid state. [1]

In this work, the top electrodes were deposited by thermal evaporation through a shadow mask to define 5 to 6 separate cells on one device. Solar cell active areas were accurately measured for each device using an optical Dino-Lite AM4113ZTL microscope.

Alq_3 was evaporated in an Edwards 306 vacuum chamber by evenly raising the temperature from 185 °C to 200 °C within 10 minutes. Final thickness of Alq_3 film was 3.7 nm.

The metal electrode was evaporated in a similar manner immediately after the evaporation of the buffer layer without opening the chamber. A small amount of silver was placed in a boat made of molybdenum, the melting point of which is one of the highest of pure metals. The solar cell after Ag evaporation is depicted in Figure 3.7.

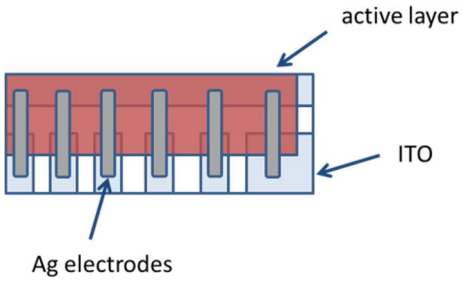

Figure 3.7. *The BHJ solar cell made in this work. The layers: white: glass, light blue: ITO, brown: organic, active layer, grey: Ag. ZnO and Alq_3 are covered by other layers in this picture.*

A structure described above, the different layers in a BHJ solar cell, is depicted in Figure 3.8.

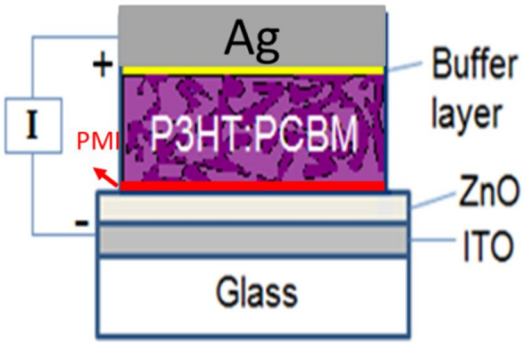

Figure 3.8. *Different layers in a BHJ solar cell.*

The description of the first set of BHJ cells experiments is presented below. The PMIs used in these cells are ZA87, ZA96 and ZA97.

ITO | ZnO | PMI | P3HT:PCBM | Alq_3 | Ag
ITO | ZnO | P3HT:PCBM | Alq_3 |Ag (reference cell not containing PMI)

The structure of the second series of BHJ cells experiments is similar to the structure of the first series, except for an attempt to optimize the concentration of the PMI ZA96. The used PMIs and concentrations in the second series were ZA96 (0.11 mM), ZA96 (0.30 mM), and ZA97 (0.11 mM).

3.2.2 Solid-state dye-sensitized solar cells (ssDSSC)

In these experiments, building solid-state dye-sensitized solar cells (ssDSSC), fluorine-doped tin oxide (FTO) was used instead of ITO. Fluorine-doped tin oxide coated glass is electrically conductive and ideal for use in a wide range of devices, including thin film photovoltaics. FTO is relatively stable under atmospheric conditions, chemically inert, mechanically hard, high-temperature resistant, has a high tolerance to physical abrasion and is less expensive than indium tin oxide (ITO).

In this work two types of commercial FTO plates were used:
- etched FTO electrodes

- scaffolding titania electrodes: etched FTO, blocking layer of TiO_2 and a scaffolding layer of mesoporous TiO_2 (600 nm).

Both were supplied by Solaronix, Switzerland.

In the solid-state dye-sensitized solar cells built in this work titanium oxide is in two layers: a hole-blocking layer and a mesoporous layer (Fig. 3.9). The dye molecules attach on the surface of TiO_2, which is porous and thus allows space for a larger amount of molecules compared to a flat surface. Porous materials are of great significance because of their ability to interact with particles not only at their surfaces but also throughout the bulk of the materials. The preparation of mesoporous materials is mainly building mesosized pore spaces, 2—50 nm, and arranging them. [54]

The commercial ruthenium dye used in this work (N719) and the four PMIs were then deposited on nanoporous TiO_2. Self-assembled monolayers of organic dyes on nanoporous TiO_2 thin films are formed by the adsorption of an active anchoring group on a solid substrate. The driving force for spontaneous formation of the SAMs, in immersing a substrate into the solution, includes chemical bond formation of the anchoring group with the surface and intermolecular interactions.

The usage of the perylene imides as sensitizers in solar cells has been discussed in chapter 2.3.3. PMI depositions and Ag evaporation were done in the same way as explained in the BHJ section.

In this work P3HT solution was prepared as follows: 20 mg P3HT in 1 ml anhydrous chlorobenzene, dissolved at 70 °C and 300 rpm for a few hours covered with folio. Each spin-coated film (size of the substrate: 2 x 2 cm) was prepared by spreading 70 µl of the P3HT solution, spinning at 2000 rpm for 30s.

The structure of a ssDSSC solar cell with layers described in the beginning of this chapter is presented in Figure 3.9.

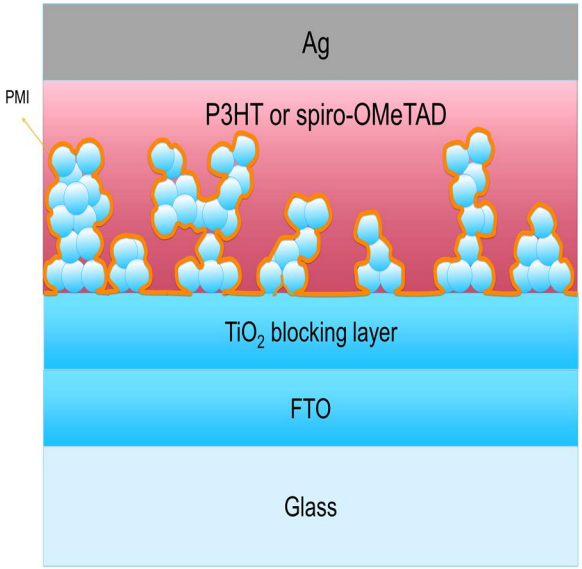

Figure 3.9. *The structure of the ssDSSC.*

The difference of the two layers of TiO_2 is visible in the middle of the picture. The blocking layer is a highly compact anatase TiO_2 layer. The mesoporous layer, above the blocking layer, is surrounded by the dye, marked by orange.

In Figure 3.10 there is an example of the energy levels of the ssDSSC constituents. There are TiO_2 as a hole-blocking layer and the energy levels of two dyes, ZA75 and ZA96 in the same picture with P3HT and spiro-OMeTAD as examples of a hole transporting material. The significance of the self-assembled monolayer of the PMI sensitizer is to retard the interfacial back electron transfer from TiO_2 conduction band to the HTM.

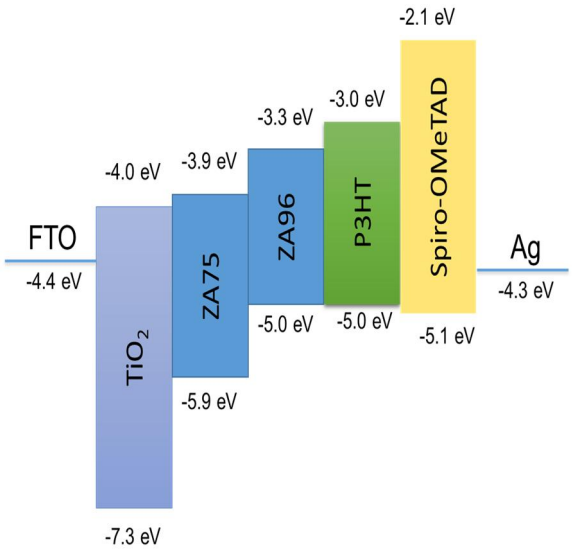

Figure 3.10. *An example of the energy levels of the constituents of a ssDSSC.*

The structure of the first series of ssDSSC experiments was:

FTO | TiO_2 b.l. | TiO_2 (600 nm) | dye | spiro-OMeTAD or P3HT | Ag

and

FTO |TiO_2 b.l. | TiO_2 (600 nm) | N719 | spiro-OMeTAD or P3HT | Ag

was used as a reference cell. The PMIs tested in this series were ZA96 and ZA97. As HTM, both Spiro-OMeTAD and P3HT were experimented with.

When spiro-OMeTAD had been used as HTM, it was necessary to combine it with bis(tri fluoromethylsulfonyl)imide (Li-TFSI) and 4-tert-butylpyridine (tBP) dopants, according to the literature. Lithium salts have been shown to dramatically increase the conductivity in a broad range of polymeric and small molecule organic semiconductors. They are required to maximize the performance and the long-term stability of ssDSSCs. [55]

The structure of the second series of ssDSSC experiments was:

FTO | TiO_2 b.l. | TiO_2 (600 nm) | dye | P3HT | Ag

and again

FTO | TiO_2 b.l. | TiO_2 (600 nm) | N719 | P3HT | Ag

was used as a reference. The PMIs used here: ZA75, ZA96 and ZA97.

The depositions of the dyes and the preparation of the P3HT layer were executed as described earlier. In these experiments spiro-OMeTAD as HTM was omitted, because P3HT seemed to work in a better way in the first series.

The structure of the third series, then, is depicted below as a two structures: in the first one the TiO_2 layers are from Solaronix (as in previous experiments) and in the second structure a home-made compact and mesoporous layers are used. The PMIs used here: ZA96 and ZA97 and N719 acts as a reference:

Solaronix | dye | P3HT | Ag and
FTO | TiO_2 b.l. | TiO_2| dye |P3HT| Ag

where Solaronix = FTO | TiO_2 b.l.| TiO_2 (600 nm) | (the same as in the first and the second series) and FTO | TiO_2 b.l. | TiO_2| = home-made compact layer, 300 nm and a mesoporous layer.

The compact layer, 300 nm, of TiO_2 was made by spin-coating 70 µl TiO_2 (Solaronix:Ti-Nanoxide-T) at 3000 rpm, for 30 s and then heating on a hot plate, 125 °C and the mesoporous TiO_2 layer by spin-coating TiO_2:ethanol 2:5, 1500 rpm, acceleration 2000 rpm/s, 45s. The expected thickness of the mesoporous TiO_2 layer was then ≈1 µm. Home-made TiO_2 plates were heated at 500 rpm for 30 min before the deposition of the dye [56].

P3HT solution in the third series was made as follows: 0,5 ml of 10 mg PHT / ml anhydrous chlorobenzene, dissolved in chlorobenzene at 50 °C overnight, covered with folio, rpm 300; then spin coating: blowing with N_2, 50 µl, left 1 minute, 30s with 2000 rpm.

The solar cells are characterized by the *I–V* measurements, performed under 1 sun illumination, which corresponds to a solar mass AM 1.5 G, an international standard for input power. The light source is a Xe lamp (66921, Newport). A 315—710 nm bandpass filter (FGS900S, Thorlabs) is adopted to select the correct wavelength area. The light intensity is calibrated to AM 1.5 G with a silicon reference cell (Oriel instruments).

Current densities both in the dark and under illumination of the adjacent electrodes of a cell (in the FTO plates there is only 1 electrode in a plate) were measured as a function of voltage in the range of -0.2—0.6 V using Agilent E5272A SMU (Source Monitor Unit). The measurements were executed one hour after the evaporation.

From the measured *I–V* curves, I_{SC}, U_{OC} and the maximum values for current and voltage, I_{max} and U_{max} were determined, and further the maximum of power, *FF* and PCE using equation 4. The surface areas of the electrodes were measured, too, in order to compare the values of current between the electrodes. The values of the power conversion efficiency are presented as an average value of all of the electrodes of the same structure and as a maximum value for a single cell.

The absorption spectrum contains valuable information of the molecular composition of the active layer and the impact of the solvent used and of the concentrations of the structures in solar cells. The absorption spectra of the ready-made samples were measured (Shimadzu UV-2501PC -spectrophotometer) in the range of 300—850 nm.

3.3 Computational models and methods

The initial ground state models of the molecules studied in this Thesis, ZA75, ZA87, ZA96, and ZA97, are presented in Figure 3.1. [34]

Density functional theory (DFT) and the time-dependent DFT (TDDFT) methods were applied using the Gaussian 09 (Revision D.01) suite of programs [56]. The ground-state geometries were optimized and the electronic properties calculated in vacuum using the PBE1PBE (*i.e.* PBE0) approximation, the combination of the pure functional of Perdew, Burke, and Ernzerhof [57] [58] as made into a hybrid by Adamo [59].

The PBE1PBE functional uses 25 % exchange and 75 % correlation weighting. The suitable level of theory was verified with the polarized split-valence basis sets 6-31G(d) and 6-311+G(d,p), the latter including also diffuse functions. The energies of the highest occupied molecular orbital (HOMO), the lowest unoccupied molecular orbital (LUMO) and the energy difference between the two were calculated at the PBE1PBE/6-311+G(d,p).

Perdew, Ernzerhof, and Burke proposed a hybrid functional PBE0 which is based on the PBE GGA functional. In a spirit of PBE, the PBE0 functional does not contain any empirically determined parameters because the 25 % of mixing is determined by theoretical reasoning on the basis of perturbation theory. [47]

4. RESULTS AND DISCUSSION

4.1 Experimental results

4.1.1 Bulk-heterojunction (BHJ) solar cells

Three of the PMIs (ZA96, ZA97 and ZA87) were adopted as an interlayer in BHJ solar cells. The energy levels of the used compounds, as derived from DPV measurements by Ahmed et al. [33] together with those of the other constituents of the BHJ solar cell, are illustrated in Figure 4.1. The desired direction of electrons/holes in the BHJ cell is guaranteed by inserting a hole-blocking layer (ZnO) between the ITO and the active layer. All the studied PMIs show suitable energy levels for electron injection to ZnO, thus being in principle suitable molecular interlayers for the BHJ solar cell structure under investigation.

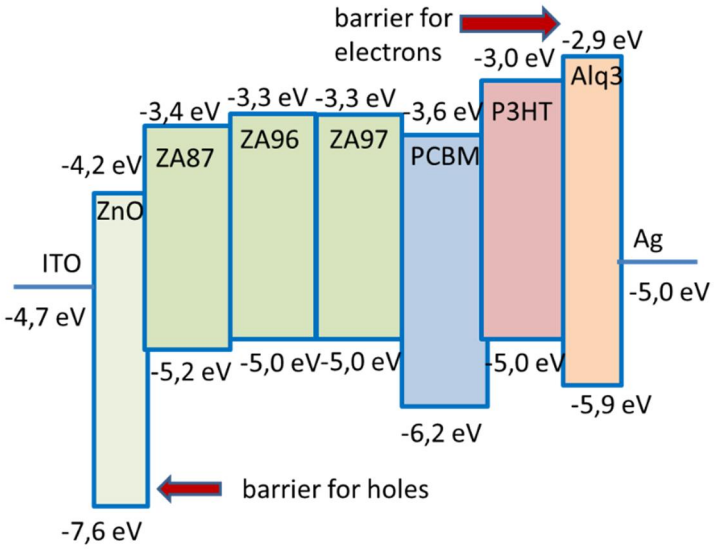

Figure 4.1. *The energy levels of the used compounds in different layers in a ITO | ZnO | PMI | donor:PCBM | Alq_3 | Ag BHJ solar cell.*

Two sets of experiments (ITO | ZnO | PMI | P3HT:PCBM | Alq_3 | Ag) were carried out, as described in chapter 3.2.1. *I–V* curves were recorded on the devices being exposed to ambient air for 1 h after the top-electrode evaporation. All the solar cells were kept in ambient condition during the fabrication and characterization, and tested without any encapsulation.

As an example, the current (*I*) vs. voltage (*V*) characteristics, recorded with 1 sun illumination, of the reference cell and of a ZA96 cell are presented in the following pictures (Figures 4.2a and 4.2b).

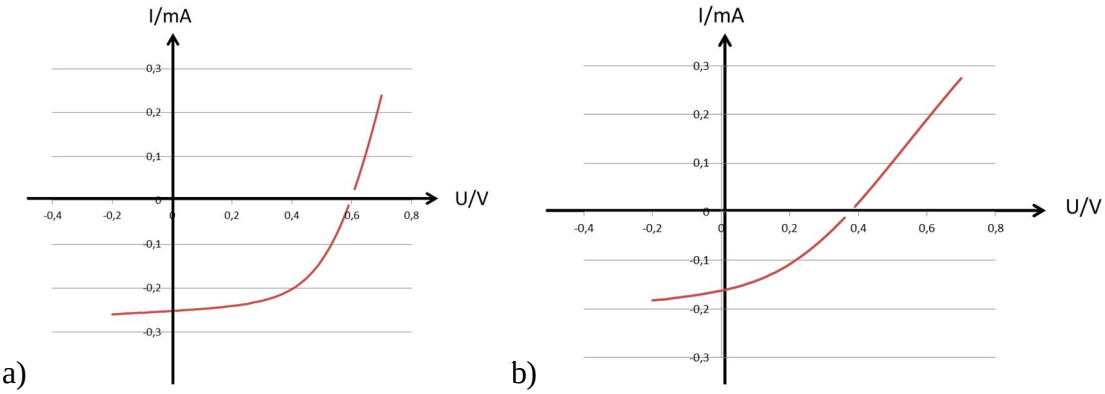

a) b)

Figure 4.2. *a) I–V curve, ITO | ZnO | P3HT:PCBM | Alq_3 |Ag (reference cell)*

b) I–V curve, ITO | ZnO | ZA96 | P3HT:PCBM | Alq_3 | Ag .

The photovoltaic parameters, derived from the recorded *J–V* curves, are presented in Table 4.1.

Table 4.1. *BHJ, combined results, 1st and 2nd series.*

sample	***I_{SC}*, mA/cm2**	***Uoc*, mV**	***FF***	***PCE*, ave %**	**PCE, best, %**
Ref	14.30	601.65	0.51	4.38 ± 0.40	4.80
ZA87	12.80	541.00	0.39	2.70[a]	2.70
ZA96	10.57	419.30	0.38	2.30 ± 1.48	4.00
ZA97	12.34	563.00	0.46	3.40 ± 0.94	4.60

ZA87 was tested in one set of solar cells (5 devices)[a], whereas several sets of cells containing either ZA96 or ZA97 had been fabricated.

The highest PCE values were obtained for the reference cells, not containing PMI. The best electrode had an efficiency over 5 %, which is the highest efficiency value ever reported in our laboratory for the same structure. Reason for this efficiency improvement compared to earlier results is most probably the fact that all the steps of the devices fabrication have been carried out in a cleanroom laboratory (ISO 6), recently built at Tampere University of Technology. Working in a cleanroom allowed the fabrication of higher quality films (more homogeneous and without pinholes), which in turn led to enhanced photovoltaic performance of the corresponding solar cells.

From Figure 4.2a and from the data in Table 4.1, it is evident that the main reason for the higher efficiency of the reference sample is the higher FF (in spite of the small increase in all the other photovoltaic parameters as well). When a PMI is added between ZnO and P3HT:PCBM, the addition of a one more interface in the cell probably worsen the contact at the hybrid organic–inorganic junction (ZnO|P3HT:PCBM), thus increasing the series

resistance of the cell. This is considered to be responsible for the reduced FF, and thus of the lower solar cell efficiency.

Among the tested PMIs, ZA97-containing cells performed best. The highest efficiency of ZA97 samples (4.6 %) was only slightly lower than the one of the reference (4.8 %) cells. For the ZA96 cells, a higher concentration of ZA96 self-assembling solution was also tested, with the aim of improving the coverage of the dye molecule onto ZnO. Unfortunately, the solar cells experiments did not lead to interesting results and were thus discarded from the Thesis. Since the addition of the PMI interlayer in BHJ cells did not appear promising in enhancing the solar cell performance, this study was not continued.

4.1.2 Solid-state dye-sensitized solar cells (ssDSSC)

In solid-state dye-sensitized solar cells (ssDSSC), ZA75, ZA96, and ZA97 were used as sensitizers. The energy levels of the studied compounds (measurements by Ahmed et. al. [33]), and of the other constituents of the ssDSSCs, are illustrated in Figure 3.10. The LUMO energy levels of PMIs, being higher than the conduction band of TiO_2 (4.2 eV), clearly show that such dyes can inject electrons to the conduction band of titanium dioxide, and can in principle show photo electron injection capabilities in ssDSSCs.

Three sets of experiments were performed (see chapter 3.2.2):
- 1st set: Solaronix | dye | spiro-OMeTAD or P3HT | Ag
- 2nd set: Solaronix | dye | P3HT | Ag
- 3rd set: Solaronix | dye | P3HT | Ag and
  FTO | TiO_2 b.l. | TiO_2 mes.| dye |P3HT| Ag (home-made blocking (b.l.) and mesoporous (mes.) layers)

In addition to the mentioned sets, a solar cell not containing any dye was also tested to evaluate the beneficial effect of PMI in the ssDSSC, and the injection of PMI to the TiO_2. For that cell (FTO| TiO_2 b.l. | TiO_2 (600 nm) | no dye | P3HT | Ag) the photovoltaic parameters extracted from current density–voltage characteristics have been determined with the following values: J_{SC} = 0.535 mAcm^{-2}, V_{OC} = 0.328 V, FF = 0.292 and PCE = 0.051 %.

In the first set of ssDSSC experiments, the calculated PCEs of the cells containing spiro-OMeTAD (Solaronix | dye | spiro-OMeTAD | Ag) were much lower compared to results with P3HT, and thus discarded. The results of the three sets with the same structure (P3HT as a HTM) and in same condition (same time of air exposure after fabrication) were averaged together, see Table 4.2. The average values of the photovoltaic parameters and the best values of PCE for a single cell of the combined results (*i.e.* 1st, 2nd and 3rd sets) are presented in Table 4.2 The corresponding, discarded results with spiro-OMeTAD are in Table 4.3.

In addition, the cells of the second set were measured twice in the solar simulator: 1 hour after the evaporation (day 0) and three days later (day 3). This was done to monitor the degradation of the devices in time. Examples of the *J–V* curves describing the time development in the second set are presented in Figures 4.3a and 4.3b. In the pictures on the left side there are the *J–V* curves in dark and under

illumination after one hour (day 0) from the evaporation of the electrodes, while in the pictures on the right side we can see the corresponding curves in the measurements after approximately three days (day 3).

The photovoltaic parameters obtained from the *J–V* curves of the second set measured after 3 days (day 3) are reported in Table 4.4, together with the averaged efficiency (two cells of each structure were built). The cells of the third series were measured three times in the solar simulator: 1 hour, 72 h and 120 h after the top-electrode evaporation. The results from all the measurements of the three series, including those to monitor the degradation, are summarized in Table 4.2.

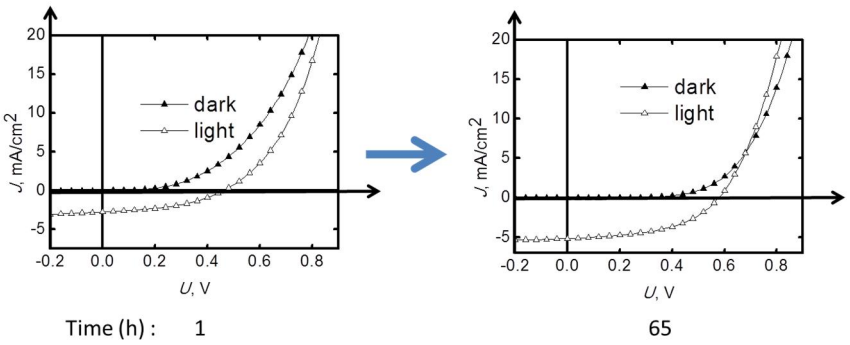

Figure 4.3 a. *J–V curve, FTO | TiO_2 b.l. | TiO_2 (600 nm)| ZA96 | P3HT | Ag.*

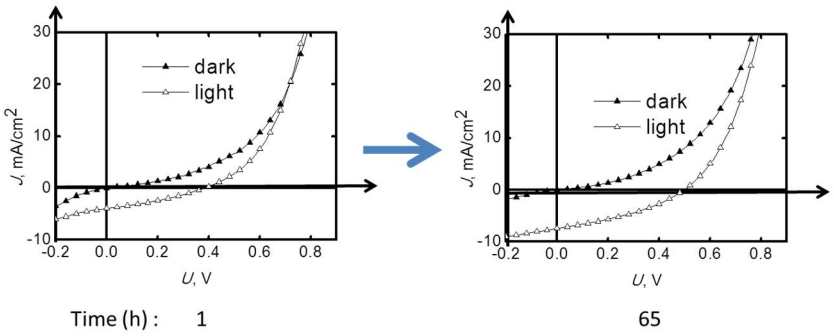

Figure 4.3 b*. J–V curve, FTO | TiO_2 b.l. | TiO_2 (600 nm) | ZA97 | P3HT | Ag.*

Table 4.2*. ssDSSC, combined results, day 0, 1st, 2nd and 3rd series.*

Dye	***Jsc*, mA/cm2**	***Uoc*, V**	***FF***	**PCE, ave %**	**PCE, best, %**
N719	5.65	0.52	0.39	1.24 ± 0.82	2.25
ZA75	1.10	0.50	0.25	0.25 ± 0.00	0.25
ZA96	3.59	0.50	0.42	0.75 ± 0.27	1.06
ZA97	3.14	0.40	0.33	0.43 ± 0.18	0.63

Table 4.3*. ssDSSC, results, day 0, 1st series,* spiro-OMeTAD as HTM .

dye	J_{SC}**, mA/cm2**	$V_{OC,}$ **mV**	***FF***	**PCE, ave %**
N719	3.12	841.24	0.48	1.30
ZA97	0.13	664.45	0.51	0.04
ZA96	0.30	663.35	0.48	0.09

Table 4.4*. ssDSSC, results, new measurements, day 3, 2nd series.*

Dye	J_{SC}**, mA/cm 2**	U_{OC}**, V**	***FF***	**PCE, ave %**	**PCE,best , %**
N719	3.35	0.62	0.38	0.80 $\pm$ 0.24	0.97
ZA75	0.78	0.51	0.47	0.19 $\pm$ 0.02	0.20
ZA96	3.91	0.57	0.49	1.09 $\pm$ 0.53	1.47
ZA97	7.17	0.48	0.35	1.21 $\pm$ 0.16	1.33

In the combined results of 1st, 2nd, and 3rd sets of measurements (Table 4.2) it can be seen that the average PCE value of ZA96 cell is the highest among those of the PMI devices. Compared to the cell without dye, with extremely poor efficiency (0.051 %), PMI cells are more efficient. The PCE values obtained in this work with ZA96 and ZA97 are 21—24 times the PCE value of the cell without dye. This proves a successful use of PMI antennas in ssDSSC devices, because of the significant increase in the cell efficiency due to the PMI. This also demonstrates the charge injection from PMI to TiO_2.

The best value of the PCE is obtained with the commercial dye N719 (2.25 %). In general, it is worth noticing quite low PCE values for all the solar cells. This may be due to the fact that our ssDSSCs are fabricated and characterized in air, without any encapsulation of the devices. Furthermore, these are the first examples of

ssDSSCs ever studied in our group. Hence, further optimization in the experimental conditions has not yet been carried out. It is well-known that the efficiency of P3HT-cells can be significantly improved by doping and annealing treatments. Moreover, the thickness of the mesoporous TiO_2 also needs optimization. Commonly, in literature a 2 µm thick mesoporous TiO_2 is supposed to maximize the incident light harvesting. [37, 60, 61]

However, a relative comparison between solar cells structures containing different dyes can be accurately done, and this represents the target of the Thesis work. Results of the photovoltaic parameters of the new measurements (day 3, 2nd set, Table 4.4) show that based on the calculated average values of the PCEs, ZA97 seems to function best, but the highest PCE value was measured with ZA96 (nearly 1.5 %). It is worth noticing that the averaged PCE values of ZA96 and ZA97 cells are higher than those measured for N719 cells, within the deviation. These ssDSSC results suggest a beneficial use of PMIs as sensitizers, particularly when ZA96 or ZA97 is adopted.

Moreover, when compared to the N719 cells performance, PMI-containing devices represent a promising alternative to the traditional rare metal -sensitized cells (Ru). In fact, finding organic sensitizers to replace Ru-dyes in the cells (such as N719) has been the focus of intense research in the latest years.

Furthermore, a tremendous increase in the PCE is obtained with devices containing our PMIs, compared to similar published solar cell architectures with other PMI anhydrides [38]. This suggests the big potential of our novel dyes as building blocks of ssDSSCs, in spite of the lack of optimization in our devices.

The improvement of the function of the second set cells with time (3 days) is to be seen in the examples of the *J–V* curves describing the time development in the second set are (Figures 4.3a and 4.3b). In the right hand side pictures the curves are better in agreement with the behavior of the ideal photodiode; the values of the short circuit current densities are also higher.

In the first measurements of the second set there were some contact problems with the electrodes; new measurements show that the PCEs of the cells containing ZA96 and ZA97 have risen remarkably. This may be due to a better contact in the electrodes, and also the oxidation of the electrode with time can affect the function of the cell by raising the work function of the Ag electrode and in that way improve the flow of charges in the desired direction.

In addition to PCE, its constituents (I_{SC}, V_{OC}, *FF*) were depicted in order to evaluate the main reason for the cell degradation. This is illustrated in Figures 4.4a—d.

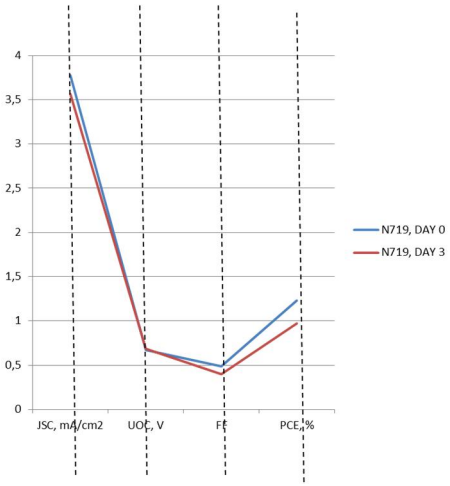

a)

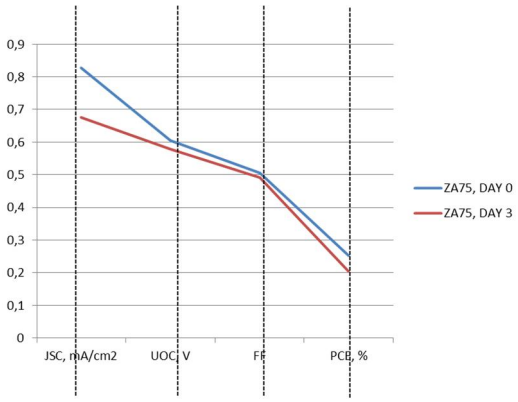

b)

Figure 4.4a and 4.4b. *I_{SC}, V_{OC}, FF and PCE, old and new measurements, N719 (a) and ZA75 (b).*

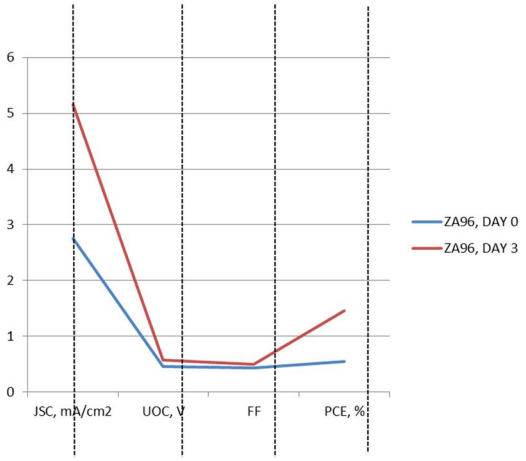

c)

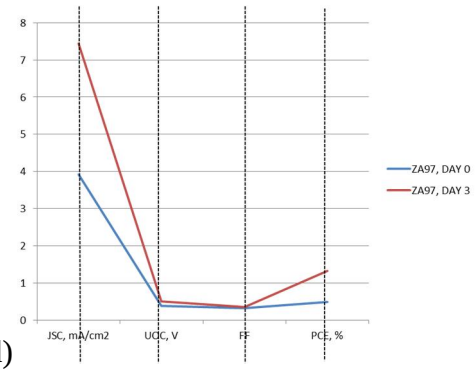

d)

Figure 4.4c and 4 .4d. *I_{SC}, V_{OC}, FF and PCE, old and new measurements, ZA96 (c) and ZA97 (d).*

It is visible in Figure 4.4a (N719) that all the values of the parameters depicted except *Uoc* have decreased. In the case of ZA75 (Figure 4.4b) all the values have decreased and comparing the values of the parameters when ZA96 or ZA97 (Figures 4.4c and d) was used, there is an increase in *Isc* and along with it an increase in the value of PCE.

4.2 Computational results

The calculated E_{HOMO}, E_{LUMO} and $E_{HOMO-LUMO}$ values are listed in Table 4.5.

Table 4.5. *Computational HOMO and LUMO energies, E_{LUMO}, E_{HOMO}, and the corresponding energy differences, $\Delta E_{(HOMO\ -LUMO)}$, (in eV) of ZA75, ZA87, ZA96, and ZA97, calculated with the PBE0 functional.*

Compound	E_{HOMO} **(eV)**	E_{LUMO} **(eV)**	$\Delta E_{(HOMO-LUMO)}$ **(eV)**
ZA75	-6.39	-3.51	2.88
ZA87	-5.84	-3.15	2.69
ZA96	-5.80	-3.28	2.52
ZA97	-5.51	-2.83	2.68

The computational energy values of the HOMO and LUMO levels of the molecules studied are represented in Figure 4.5, together with the experimental HOMO and LUMO energies, previously obtained from the DPV data [33].

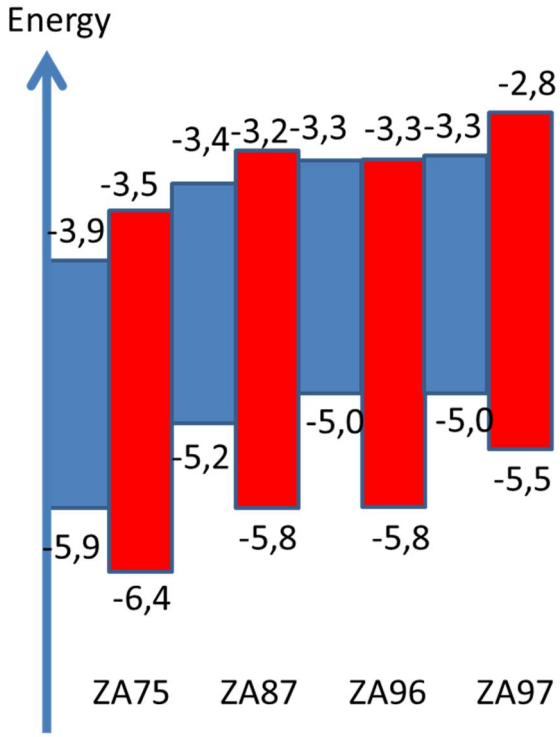

Figure 4.5. *The experimental (blue) [33] and computational (red) values of the HOMO (lower) and LUMO (upper) levels of the molecules studied.*

The computational HOMO values of the PMIs seem to be distinctly lower than the experimental values. Nonetheless, the general trend, when the HOMO and LUMO levels are compared, is approximately the same, except for ZA96 and ZA97, where there is a difference in the computational values, while the experimental values are the same.

The orbital spatial distributions of HOMO (on the left) and LUMO (on the right) for the four PMIs are shown in Figure 4.6.

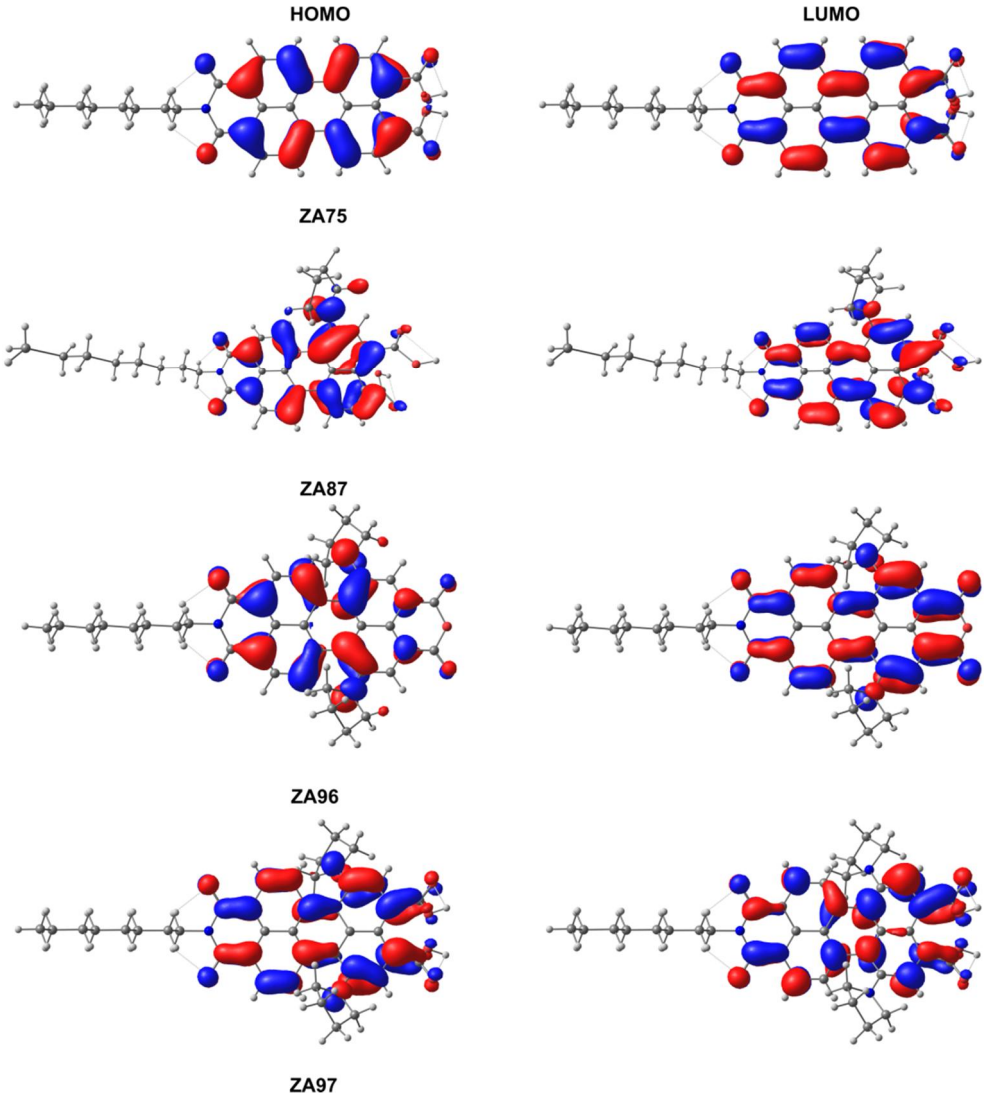

Figure 4.6. *The frontier orbitals of the PMIs studied. Figure made by T. I. Hukka.*

In the case of ZA75 the electron density in both HOMO and LUMO is evenly distributed on the PMI ring, whereas in the case of ZA87 the electron density is slightly oriented towards the pyrrolidine substituent. In ZA96 and ZA97 the HOMO and LUMO are, in addition, distributed towards the anhydride or diacid ends of the molecules.

5. CONCLUSIONS

In the BHJ experiments, the PMIs were expected to act as an interlayer at the organic–inorganic interface of the solar cells, *i.e.* to direct the electrons towards the anode and the holes towards the bulk layer. However, the photovoltaic parameters derived from the current–voltage characteristics of the cells show that the introduction of PMI seems to worsen the device performance. Some kinds of traps may be formed, or the PMI layer acts as an insulating barrier, sorting the charges not in the expected way. In BHJ structures, the LUMO levels of the tested PMIs are rather high, higher than the LUMO level of PCBM (see Fig. 4.1), which may also be an obstacle for the electron flow in the cell.

Significant improvements in the efficiencies were achieved, when comparing the performance of the reference solar cell, which did not contain PMI, to earlier results carried out in the same laboratory. The high quality of the films, prepared in a cleanroom laboratory recently built at TUT, is expected to be the main reason for the development of devices with enhanced performance. However, the study concerning PMIs as interlayer in BHJ cells was not continued further, due to the lack of promising results.

As for the ssDSSC experiments, the capability of the PMIs used in this work to act as sensitizers, *i.e.*to inject electrons to the titanium dioxide, was successfully demonstrated. In fact, a 20-times increase in the PCE of the ssDSSCs was achieved thanks to the addition of the PMI. Furthermore, for two of the PMI cell-structures presented in this work, the PCE values were comparable to those obtained for the device adopting a well-known and mostly used commercial ruthenium dye, N719. This suggests the beneficial use of the PMIs studied in this Thesis in ssDSSCs as a potential replacement for the expensive rare metal ruthenium-containing dyes as modifiers of the TiO_2 surfaces.

As a necessary future work a further optimization of the experimental conditions (doping and annealing treatments, thickness of the mesoporous TiO_2, PMI deposition conditions, etc.) would be essential, in order to enhance the overall efficiency of the solar cells. Although the optimization in our devices was not done yet, PMIs with electron donating groups, such as ZA97 and ZA96, are promising dyes for efficient ssDSSCs.

The degradation in time of the photovoltaic devices was also studied for some of the samples: the PCEs of the ssDSSCs containing ZA96 and ZA97 almost tripled in three days. The possible reasons for this were discussed in chapter 4.1.2.

Finally, comparing the results from the experiments (DPV measurements) and the modeling (DFT calculations), it can be noted that the experimental LUMO values of ZA75, ZA87 and ZA97 are a bit lower than the corresponding calculated values. However, the energy levels are qualitatively the same, if the energy diagram of the whole cell is considered (Fig. 4.1 and Fig. 3.10). In other words, the computational results confirm the electron injection capabilities of these PMI dyes to the conduction band of titanium dioxide.

REFERENCES

[1] P. Vivo, Multilayered Thin Films for Organic Photovoltaics, Thesis for the degree of Doctor of Science in Technology, Tampere University of Technology, 2010, ISBN 978-952-15-2450-9.

[2] S. A. Kalogirou, Solar Energy Engineering—Processes and Systems; 2nd edition, Academic Press, 2014, ISBN: 978-0-12-397270-5.

[3] F. Gao, S. Ren, J. Wang, The renaissance of hybrid solar cells: progresses, challenges, and perspectives. Energy Environ. Sci., 2013, 6, 2020.

[4] U. Mehmood, S. Rahman, K. Harrabi, I. A Hussein and B. V. S. Reddy**,** Recent Advances in Dye Sensitized Solar Cells. Advances in Materials Science and Engineering, Volume 2014, Article ID 974782, 12 pages.

[5] M.-S Kim, Understanding Organic Photovoltaic Cells: Electrode, Nanostructure, Reliability, and Performance, A dissertation submitted in partial fulfillment of the requirements for the degree of Doctor of Philosophy (Materials Science and Engineering) in The University of Michigan, 2009.

[6] H. Wonneberger, Light Harvesting and Orbital Tuning Perylene Monoimides and Diimides for Photovoltaic Purposes, Dissertation zur Erlangung des Grades "Doktor der Naturwissenschaften" im Promotionsfach Chemie am Fachbereich Chemie, Pharmazie und Geowissenschaften der Johannes Gutenberg-Universität in Mainz, 2012.

[7] K. Stranius, Photochemistry of Self-Assembled Donor-Acceptor Architectures for Photoactive Supramolecular Devices, Thesis for the degree of Doctor of Philosophy, Tampere University of Technology, 2014, ISBN 978-952-15-3412-6.

[8] G. Guidetti, Photoinduced electron transfer at the interface of semiconductor and organic donor-acceptor layer, Master of Science Thesis, Tampere University of Technology, 2013.

[9] A. M. Bagher, Comparison of Organic Solar Cells and Inorganic Solar Cells, International Journal of Renewable and Sustainable Energy. Vol. 3, No. 3, 2014, pp. 53-58. doi: 10.11648/j.ijrse.20140303.12.

[10] M. Wright, A. Uddin, Organic–inorganic hybrid solar cells: A comparative review, Solar Energy Materials & Solar Cells 107, 2012, 87–111.

[11] M.C. Scharber, N.S. Sariciftci, Efficiency of bulk-heterojunction organic solar cells, Progress in Polymer Science, 38, 2013, 1929–1940.

[12] X. Liu, H. Chen, S. Tan, Overview of high-efficiency organic photovoltaic materials and devices, Renewable and Sustainable Energy Reviews 52, 2015, 1527–1538.

[13] X. Fan, M. Zhang, X. Wang, F. Yang, X. Meng, Recent progress in organic–inorganic hybrid solar cells, J. Mater. Chem. A, 2013, 1, 8694.

[14] M. Gruber, B.A. Stickler, G. Trimmel, F. Schürrer, K. Zojer, Impact of energy alignment and morphology on the efficiency in inorganic–organic hybrid solar cells, Organic Electronics 11, 2010, 1999–2011.

[15] Y. Cao, Y. Bai, Q. Yu, Y. Cheng, S. Liu, D. Shi, F. Gao, P. Wang, Dye-sensitized solar cells with a high absorptivity ruthenium sensitizer featuring a 2-(hexylthio) thiophene conjugated bipyridine, The Journal of Physical Chemistry C 113, 2009, 6290-6297.

[16] A. Yella, H. Lee, H. Tsao HN, C. Yi, A. K. Chandira, M.K. Nazeeruddin, E.W. Dia, C.Y. Yeh, S. M. Zakeeruddi, M. Grätzel, Porphyrin-sensitized solar cells with cobalt (II/III)-based redox electrolyte exceed 12 percent efficiency, Science, 2011, 334, 629-634.

[17] J. A. Mikroyannidis, M. M. Stylianakis, P. Suresh, M. S. Roy and G. D. Sharma, Synthesis of perylene monoimide derivative and its use for quasi-solid-state dye-sensitized solar cells based on bare and modified nano-crystalline ZnO photoelectrodes, Energy Environ. Sci., 2009, 2, 1293–1301.

[18] J. Wu, Z. Lan, J. Lin, M. Huang, Y. Huang, L. Fan, G. Luo, Electrolytes in Dye-Sensitized Solar Cells, Chem. Rev. 2015, 115, 2136 – 2173.

[19] B. Li, L. Wang, B. Kang, P. Wang, Y. Qiu, Review of recent progress in solid-state dye-sensitized solar cells, Solar Energy Materials & Solar Cells 90, 2006, 549–573.

[20] A. Abrusci, S. D. Stranks, P. Docampo, H. Yip, A. K.-Y Jen, H. J., Snaith, High-performance Perovskite-Polymer Hybrid Solar Cells via Electronic Coupling with Fullerene Monolayers. Oxford–Seattle, Nano Lett., 2013, 13,3124-3128.

[21] M. A. Green, A. Ho-Baillie, H. J., Snaith, The emergence of perovskite solar cells, Nature Photonics, 2014, 8, 506–514.

[22] D. Gupta, S. Mukhopadhyay, K.S. Narayan, Fill factor in organic solar cells, Solar Energy Materials & Solar Cells, 2010, 94, 1309– 1313.

[23] V. Manninen, Molecular Modifications of Active and Anode Buffer Layers of Bulk Heterojunction Solar Cell, Thesis for the degree of Doctor of Science in Technology at Tampere University of Technology, 2014, ISBN 978-952-15-3293-1.

[24] F. Diao, W. Liang, F. Tian,Y. Wang, P. Vivo, A. Efimov, and H. Lemmetyinen, Preferential Attachments of Organic Dyes onto {101} Facets of TiO_2 Nanoparticles, J. Phys. Chem. C, 2015, 119 (16), 8960–8965.

[25] P.Lellig, M. A. Niedermeier, M.a Rawolle, M. Meister, F. Laquai, P. M*ü*ller-Buschbaum and J. S. Gutmann, Comparative study of conventional and hybrid blocking layers for solid-state dye-sensitized solar cells, Phys. Chem. Chem. Phys., 2012, 14, 1607–1613.

[26] F. Matteocci, G. Mincuzzi, F. Giordano, A. Capasso, E. Artuso, C. Barolo, G. Viscardi,T.M. Brown, A. Reale, A. Di Carlo, Blocking layer optimisation of poly(3-hexylthiopene) based Solid State Dye Sensitized Solar Cells, Organic Electronics, 2013, 14, 1882–1890.

[27] D. H. Wang, P. Morin, C. Lee, A. Ko Ko Kyaw, M. Leclerc and A. J. Heeger, Effect of processing additive on morphology and charge extraction in bulk-heterojunction solar cells, J. Mater. Chem. A, 2014, 2, 15052.

[28] L. B. Roberson, M. A. Poggi, J. Kowalik, G. P. Smestad, L. A. Bottomley, L. M. Tolbert, Correlation of morphology and device performance in inorganic–organic TiO_2–polythiophene hybrid solid-state solar cells, Coordination Chemistry Reviews, 2004, 1491–1499.

[29] C.-K. Lee, C.-W. Pao, C.-W. Chen, Correlation of nanoscale organizations of polymer and nanocrystals in polymer/inorganic nanocrystal bulk heterojunction hybrid solar cells: insights from multiscale molecular simulations, Energy Environ. Sci., 2013, 6, 307.

[30] M. C. Scharber, D. Mühlbacher, M. Koppe, P. Denk, C. Waldauf, A. J. Heeger, C. J. Brabec, Design Rules for Donors in Bulk-Heterojunction Solar Cells—Towards 10 % Energy-Conversion Efficiency, Adv. Mater., 2006, 18, 789 –794.

[31] H. Xiang, S.-H. Wei, X. Gong, Identifying optimal inorganic nanomaterials for hybrid solar cells, The Journal of Physical Chemistry C, 2009, 113, 18968–18972.

[32] C. Li, H. Wonneberger, Perylene Imides for Organic Photovoltaics: Yesterday, Today, and Tomorrow, Advanced Materials, 2012, 24, 5– 7.

[33] Z. Ahmed, L. George, A. Hiltunen, H. Lemmetyinen, T. Hukka, A.Efimov, Synthesis and Study of Electrochemical and Optical Properties of Substituted Perylenemonoimides in Solutions and on Solid Surfaces, J. Mater. Chem. A, 2015. DOI*:* 10.1039/C5TA02241j.

[34] ACD/ChemSketch™, the ACD/ChemSketch 2012 Release (Build 51083, 28 Sep 2011), 1996–2015 Advanced Chemistry Development, Inc. 8 King Street East, Suite 107, Toronto, Ontario, Canada M5C 1B5. <http://www.acdlabs.com/company/terms.php>.

[35] M. Wang, X. Wang, P3HT/ZnO bulk-heterojunction solar cell sensitized by a perylene derivative, Sol. Energy Mater. Sol. Cells, 2008, 92, 766.

[36] M.Wang, X. Wang, P3HT/TiO_2 bulk-heterojunction solar cell sensitized by a perylene derivative, Solar Energy Materials & Solar Cells 91, 2007, 1782–1787.

[37] I. A. Howard, M. Meister, B. Baumeier, H. Wonneberger, N. Pschirer, R. Sens, I. Bruder, C. Li, K. Müllen, D. Andrienko, F. Laquai, Two Channels of Charge Generation in Perylene Monoimide Solid-State Dye-Sensitized Solar Cells, Advanced Energy Materials, 2014, Volume 4, Issue 2, January 28.

[38] S. Erten-Ela, G. Turkmen, Perylene imide dyes for solid-state dye-sensitized solar cells: Spectroscopy, energy levels and photovoltaic performance, Renewable Energy, 2011, 36, 1821-1825.

[39] C. Zafer, C. Karapire, N. S. Sariciftci, S. Icli, Characterization of *N, N'*-bis-2-(1-hydroxy-4-methylpentyl)-3, 4, 9, 10-perylene bis(dicarboximide) sensitized nanocrystalline TiO_2 solar cells with polythiophene hole conductors, Solar Energy Materials & Solar Cells, 2005, 88, 11–21.

[40] J. Fortage, M. S*é*verac, C. Houarner-Rassin, Y. Pellegrin, E. Blart, F. Odobel, Synthesis of new perylene imide dyes and their photovoltaic performances in nanocrystalline TiO_2 dye-sensitized solar cells, Journal of Photochemistry and Photobiology A: Chemistry, 2008, 197, 156–169.

[41] Y. Shibano, T. Umeyama, Y. Matano, H. Imahori, Electron-Donating Perylene Tetracarboxylic Acids for Dye-Sensitized Solar Cells, Organic Letters 2007, Vol. 9, No. 10, 1971 – 1974.

[42] J. A. Hauch, P.l Schilinsky, S. A. Choulis, R. Childers, M. Biele, C. J. Brabec, Flexible organic P3HT:PCBM bulk-heterojunction modules with more than 1 year outdoor lifetime, Solar Energy Materials&Solar Cells, 2008, 92, 727–731.

[43] M. S. White, D. C. Olson, S. E. Shaheen, N. Kopidakis and D. S. Ginley, Inverted bulk-heterojunction plastic solar cells, Appl. Phys. Lett., 2006, 89, 143517–143520.

[44] P. Atkins, R. Friedman: Molecular Quantum Mechanics, Oxford University Press, 2005, ISBN-13: 978-0199541423.

[45] W. Koch, M. C. Holthausen, A Chemist's Guide to Density Functional Theory, Wiley-VCH Verlag GmbH, 2001, ISBNs: 3-527-30372-3 (Softcover); 3-527-60004-3 (Electronic).

[46] V. Manninen, M. Niskanen, T. I. Hukka, F. Pasker, S. Claus, S. Höger, J. Baek, T. Umeyama, H. Imahori, H. Lemmetyinen, Conjugated donor–acceptor (D–A) copolymers in inverted organic solar cells — a combined experimental and modelling study, J. Mater. Chem. A, 2013, 1, 7451.

[47] P. Aittala: Computational study of Charge transfer in a Porphirine–Quonone Complex and Novel akoxypyridylindolizine Derivatives; Thesis for the degree of Doctor of Science in Technology at Tampere University of Technology, 2010, ISBN 978-952-15-2479-0.

[48] T. Toivonen: Computational study of Photoinduced Energy Transfer of Porphyrin–Fullerene and Oligo(p-phenyenevinylene)–Fullerene Dyads, Thesis for the degree of Doctor of Philosophy, Tampere University of Technology, 2007, ISBN 978-952-15-1883-6.

[49] T. Mohr, V. Aroulmoji, R. Samson Ravindran, M. Müller, S. Ranjitha, G. Rajarajan, P.M. Anbarasan , DFT and TD-DFT study on geometries, electronic structures and electronic absorption of some metal free dye sensitizers for dye

sensitized solar cells , Spectrochimica Acta Part A: Molecular and Biomolecular Spectroscopy, 2015, 135, 1066–1073.

[50] S. S. Kumar, P. Venkateswarlu, V. R. Rao, G.N. Rao, Synthesis, characterization and optical properties of zinc oxide nanoparticles, International Nano Letters 2013, 3:30.

[51] Solar cells that mimic plants, Nature photonics | VOL 5 | MAY 2011 |.

[52] P. Vanlaeke, A. Swinnen, I. Haeldermans, G. Vanhoyland,T. Aernouts, D. Cheyns, C. Deibel, J. D'Haen, P. Heremans, J. Poortmans, J.V. Manca, P3HT/PCBM bulk heterojunction solar cells: Relation between morphology and electro-optical characteristics, Solar Energy Materials & Solar Cells, 2006, 90 2150–2158.

[53] E. Lehtonen, Peryleenidi-imidi–fullereenidyadin synteesi ja toiminta orgaanisessa aurinkokennossa, Master of Science Thesis, Tampere University of Technology, 2013.

[54] W. Li, Z. Wu, J. Wang, A. A. Elzatahry, and D. Zhao, A Perspective on Mesoporous TiO_2 Materials, Chem. Mater., 2014, 26, 287 – 298.

[55] A. Abate,T. Leijtens, S. Pathak, J. Teuscher, R. Avolio, M. E. Errico, J. Kirkpatrik, J. M. Ball, P. Docampo, I. McPherson and H. J. Snaith, Lithium salts as ''redox active'' p-type dopants for organic semiconductors and their impact in solid-state dye-sensitized solar cells, Phys. Chem. Chem. Phys., 2013, 15, 2572.

[56] Gaussian 09, Revision D.01, M. J. Frisch, G. W. Trucks, H. B. Schlegel, G. E. Scuseria, M. A. Robb, J. R. Cheeseman, G. Scalmani, V. Barone, B. Mennucci, G. A. Petersson, H. Nakatsuji, M. Caricato, X. Li, H. P. Hratchian, A. F. Izmaylov, J. Bloino, G. Zheng, J. L. Sonnenberg, M. Hada, M. Ehara, K. Toyota, R. Fukuda, J. Hasegawa, M. Ishida, T. Nakajima, Y. Honda, O. Kitao, H. Nakai, T. Vreven, J. A. Montgomery, Jr., J. E. Peralta, F. Ogliaro, M. Bearpark, J. J. Heyd, E. Brothers, K. N. Kudin, V. N. Staroverov, R. Kobayashi, J. Normand, K. Raghavachari, A. Rendell, J. C. Burant, S. S. Iyengar, J. Tomasi, M. Cossi, N. Rega, J. M. Millam, M. Klene, J. E. Knox, J. B. Cross, V. Bakken, C. Adamo, J. Jaramillo, R. Gomperts, R. E. Stratmann, O. Yazyev, A. J. Austin, R. Cammi, C. Pomelli, J. W. Ochterski, R. L. Martin, K. Morokuma, V. G. Zakrzewski, G. A. Voth, P. Salvador, J. J. Dannenberg, S. Dapprich, A. D. Daniels, Ö. Farkas, J. B. Foresman, J. V. Ortiz, J. Cioslowski, and D. J. Fox, Gaussian, Inc., Wallingford CT, 2009.

[57] J. P. Perdew, K. Burke, and M. Ernzerhof, Generalized gradient approximation made simple, Phys. Rev. Lett., 1996, 77, 3865-68.

[58] J. P. Perdew, K. Burke, and M. Ernzerhof, Errata: Generalized gradient approximation made simple, Phys. Rev. Lett., 78 (1997) 1396.

[59] C. Adamo and V. Barone, Toward reliable density functional methods without adjustable parameters: The PBE0 model, J. Chem. Phys., 1999, 110, 6158-69.

[60] R. Zhu, C-Y. Jiang, B. Liu, S. Ramakrishna, Highly Efficient Nanoporous TiO_2-Polythiophene Hybrid Solar Cells Based on Interfacial Modification Using a Metal-Free Organic Dye, Adv. Mater., 2009, 21, 994-1000.

[61] L. Yang, U. B. Cappel, E. L. Unger, M. Karlsson, K. Karlsson, E. Gabrielsson, L. Sun, G. Boschloo, A. Hagfeldt, E. M. J. Johansson, Comparing spiro-OMeTAD and P3HT hole conductors in efficient solid state dye-sensitized solar cells, Phys. Chem. Chem. Phys., 2012, 14, 779–789.